NASA Technical Memorandum 84270

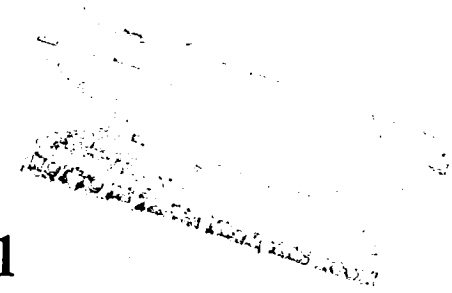

A Flight-Test and Simulation Evaluation of the Longitudinal Final Approach and Landing Performance of an Automatic System for a Light Wing Loading STOL Aircraft

Stuart C. Brown, Gordon H. Hardy,
and William S. Hindson

JUNE 1983

25th Anniversary
1958-1983

NASA

NASA Technical Memorandum 84270

A Flight-Test and Simulation Evaluation of the Longitudinal Final Approach and Landing Performance of an Automatic System for a Light Wing Loading STOL Aircraft

Stuart C. Brown, Gordon H. Hardy,
and William S. Hindson
Ames Research Center
Moffett Field, California

National Aeronautics
and Space Administration

**Scientific and Technical
Information Branch**

1983

TABLE OF CONTENTS

NOMENCLATURE

a_x, a_z	aircraft accelerations in body axis directions, g
CMN	MLS control motion noise
DME	distance-measuring equipment
g	acceleration due to gravity, m/sec^2
GPIP	glidepath intercept point
h_{rw}	aircraft altitude, relative to main wheels, measured by radio altimeter
IC_o	initial condition on dynamic element in flare guidance system at flare initiation
ICAO	International Civil Aviation Organization
ILS	instrument landing system
LWL	light wing loading
MLS	microwave landing system
N	number of samples in a group
P.C.	MLS antenna electronic phase center
PFE	MLS path-following error
P_e	probability of exceedance of a value of a random variable
q	pitch body angular rate, rad/sec
$\bar{q}$	dynamic pressure, n/M^2 (psf)
R	MLS range (DME), m
rms	root mean square
rss	root summed square
s	Laplace operator, sec^{-1}
SAS	stability augmentation system
TACAN	tactical air navigation system providing bearing and distance information
V_c	calibrated airspeed, knots
V_G	filtered ground speed, knots
x,y,z	rectangular coordinate system oriented with respect to runway; x origin is at the MLS elevation P.C., m
x_{el}, y_{el}, z_{el}	location of MLS elevation P.C., m
x_{az}, z_{az}	location of MLS azimuth P.C., m
δ_e	elevator position, deg
δ_t	throttle position, cm
θ	pitch attitude angle, deg
θ_{eng}	pitch attitude angle when servo actuators engaged
θ_n	MLS conical elevation angle, deg
μ	mean value of a random variable
σ	standard deviation of a random variable
σ_a	rms of standard deviations obtained along the final approach path from a set of approaches
$2\sigma_p$	symmetrical range of a random variable about a nominal for which the $P_e \leqslant 4.5\%$
σ_t	rms of standard deviations of total (unfiltered) MLS noise obtained along the final approach path from all approaches
ψ_n	MLS planar azimuth angle, deg
ω	natural frequency, rad/sec
$(\hat{\ })$	filtered value

Subscript

0	condition at flare initiation
td	touchdown
cg	aircraft center of gravity

A FLIGHT-TEST AND SIMULATION EVALUATION OF THE LONGITUDINAL FINAL APPROACH AND LANDING PERFORMANCE OF AN AUTOMATIC SYSTEM FOR A LIGHT WING LOADING STOL AIRCRAFT

Stuart C. Brown, Gordon H. Hardy, and William S. Hindson

Ames Research Center

As part of a comprehensive flight-test program of STOL operating systems for the terminal area being conducted at the NASA Ames Research Center, an automatic landing system has been developed and evaluated for a light wing loading turboprop aircraft. The aircraft utilized an onboard advanced digital avionics system. Flight tests were conducted at a facility that included a STOL runway site with a microwave landing system.

Longitudinal flight-test results were presented and compared with available (basically CTOL) criteria. These comparisons were augmented by results from a comprehensive simulation of the controlled aircraft which included representations of navigation errors that were encountered in flight and atmospheric disturbances.

Acceptable performance on final approach and at touchdown was achieved by the autoland (automatic landing) system for the moderate winds and turbulence conditions encountered in flight. However, some touchdown performance goals were marginally achieved, and simulation results suggested that difficulties could be encountered in the presence of more extreme atmospheric conditions. Suggestions were made for improving performance under those more extreme conditions.

An investigation utilizing flight-test results, augmented by simulation results, of an automatic landing system for a light wing loading (LWL) short takeoff and landing (STOL) aircraft was conducted at the NASA Ames Research Center. The investigation was part of a general program at the Center to determine the technology and operational requirements for STOL operations. This portion of the program was intended to provide a data base and foundation for the development of STOL criteria for the automatic control of this type of aircraft flying curved, descending flightpaths to touchdown. An airborne system, consisting of a digital computer and a set of electronic displays (known as STOLAND, ref. 1), was installed on a Twin Otter aircraft. A basic set of navigation, guidance, and control functions designed for automatic flight control and for driving the displays was implemented on the computer. Powered actuators were provided for all conventional controls as well as for a set of wing spoilers. Performance with spoilers will be described in a subsequent report.

Design concepts for the automatic control of the aircraft on final approach and touchdown were further investigated in a simulation study reported in reference 2. An analog simulation, capable of fast repetitive operation of the controlled aircraft and a wide range of atmospheric and navigational disturbances, was implemented. The fast time capability allowed ensemble statistical evaluations of performance for the more promising designs. The study indicated that performance compatible with Category III operations onto STOL runways could be obtained. A number of these concepts were incorporated as part of the airborne systems used in the flight-test program.

The purpose of this report is to describe and evaluate the longitudinal flight performance of the automatically controlled aircraft on final approach and touchdown using conventional elevator and throttle controls. The performance elements assessed include overall tracking accuracy, navigation requirements, environmental effects, ride quality, and control activity. The evaluation of flight results was augmented by results from a comprehensive digital simulation of the controlled aircraft. This simulation was designed for airborne software development, final design, and validation, and was operated concurrently with the flight tests. The simulation results allowed further delineation of the effects of atmospheric disturbances and microwave landing system (MLS) errors on system performance beyond that which could be obtained from the flight tests. The digital simulation incorporated more nonlinear effects than were implemented in the simulation used in reference 2 and therefore could represent a wider range of flight conditions; however, it operated in real time so that only smaller sets of results could be generated.

After a review of related investigations and a discussion of autoland (automatic landing) characteristics for this type of aircraft, the report describes the pertinent airborne navigation, guidance, and control systems implemented. Then, a review and assessment of available performance criteria for autoland systems is given. Next, results are presented describing the atmospheric conditions and navigational accuracies encountered during the flight tests. Finally, flight-test results are given for the final approach and touchdown and are compared with applicable criteria. Comparisons using pertinent simulation results are also included.

BACKGROUND AND HISTORY

The development of STOL transportation systems for linking metropolitan centers and smaller communities has been in progress for a number of years. These systems incorporate STOL aircraft which can make steep curved approaches into and departures from small STOLports (airports with short takeoff and landing strips) located close to metropolitan centers. These paths are constructed to achieve noise abatement, obstacle clearance, and avoidance of other types of air traffic. The MLS being introduced provides the broad horizontal and vertical coverage (as well as signals relatively free of multipath) needed for the aircraft to follow the final portions of these paths under instrument-weather conditions. For commuter service, these STOL systems can make a significant reduction in total transit time between metropolitan centers through the use of close-in STOLports rather than outlying major hub airports.

Generally, STOL aircraft are designed for high-lift capability either through the use of LWL and an extensive mechanical flap system or through a form of powered lift. The LWL aircraft is generally considered to have more limited STOL performance and is limited to shorter range missions because of its slower cruise speed. However, the LWL airplane does have the advantage of simplicity and lower fuel consumption. It is attractive for moderate-length computer operations such as the 322-km (200-mile) route between Boston and Manhattan as proposed in reference 3.

In recent years, a number of flight-demonstration programs for turboprop-powered LWL aircraft have taken place. A Twin Otter flight-test program was conducted by the FAA to compare performance for several navigational landing aid geometries on final approach and touchdown (ref. 4). Manual control with a flight director was used to fly approaches to a decision height as low as 30.5 m. A STOL flight-demonstration program was conducted by the Canadian Air Transportation Administration (CATA) to demonstrate and evaluate a complete STOL transportation system using Twin Otter aircraft (refs. 5 and 6). STOLports for this demonstration were established in Montreal and Ottawa and equipped with MLS to permit steep STOL approaches to be made under instrument-flight conditions. Manual approaches with a flight director to a 91.4-m (300-ft) decision height were flown routinely during an extensive commercial demonstration period.

As part of the recent increase in commuter airline operations, the LWL STOL transport is emerging as a highly successful concept. For example, the de Havilland DHC-7 is being used to fly from Philadelphia to Washington, D.C. (ref. 7). At Washington National Airport, dedicated STOL approach paths are flown to a separate runway that intersects the main CTOL runway. Simultaneous STOL and CTOL approaches are conducted with the STOL traffic stopping short of the main runway. Because of the proximity of the STOL runway to the CTOL runway, and the lack of a dedicated STOL navigational landing aid, simultaneous approaches were initially being conducted only in visual conditions, that is, a ceiling of at least 305 m and visibilities equal to or greater than 4.8 km (3 miles). Actual instrument capability, following installation of an MLS and further operational experience, is expected to be achieved in the future.

The advent of the STOL airplane and the MLS creates a need to examine certification and operating requirements for these systems, since they may differ from those for CTOL aircraft. The need for different requirements is reflected in the special conditions used for certification of the de Havilland DHC-7 when making STOL approaches (ref. 8). Other evaluations of STOL requirements have included (1) an investigation of airworthiness requirements for powered-lift vehicles in the powered-lift regimes of final approach, flare, and takeoff (ref. 9) and (2) a proposed procedure for relating STOL aircraft performance to runway-length requirements (ref. 10).

Another aspect of STOL aircraft performance is passenger ride comfort. Ride comfort is of particular importance to LWL aircraft because of their sensitivity to atmospheric disturbances. The subject of ride comfort has been extensively investigated through the use of motion simulators and aircraft (ref. 11), although definitive results have been difficult to obtain. One study used results from test subjects riding in aircraft to develop aircraft ride comfort criteria based on motion variables and cabin noise (ref. 12); these criteria were applied to and compared with the CATA STOL demonstration program results. A further study incorporated a broader range of variables into the ride comfort criteria (ref. 13). Inclusion of this broader range into the same ride comfort rating scale served to reduce that portion which could be allocated to aircraft motion.

In order for STOL aircraft to maintain schedules under all weather conditions, an autoland capability will ultimately be needed. Previous automatic control studies for LWL aircraft have focused on systems for minimizing turbulence response and improving ride quality (e.g., ref. 14), and improving terminal-area tracking performance (ref. 15). However, a complete autoland system for this type of aircraft has not been investigated. An autoland system designed for an LWL STOL aircraft encounters problems somewhat different from CTOL aircraft mainly during the flare maneuver. Differences may also occur during glide slope track. However, if a CTOL safety margin requiring that an approach speed 30% greater than stall speed is imposed, then the design for path and airspeed control on the final approach for the LWL STOL aircraft becomes similar to that for CTOL aircraft. This requirement usually results in the aircraft being operated on the conventional front side of the power-required-versus-airspeed curve with the speed controlled by the throttle and the flightpath controlled by the elevator. In any case, the steeper approach angle for the STOL aircraft results in operating with low trim power. The steepness of the angle is limited

by the need for an adequate power reduction margin to make airspeed adjustments.

Because of the light wing loading, the aircraft is more susceptible to atmospheric disturbances than conventional jet aircraft; hence, adequate path control and ride quality are potentially more difficult to achieve. For the flare manuever, atmospheric disturbances have an even greater effect because of the need for more precise touchdown control. The steep STOL approach angle also makes the flare maneuver more difficult. Depending on the final-approach trim attitude, the ground effect, and other factors, the aircraft may need to be rotated an even greater amount than the final-approach glide slope in order to achieve a satisfactory touchdown attitude. In addition, the low power setting at flare entry complicates adequate power and corresponding speed reduction (which interacts with pitch attitude change) during the flare maneuver. The problem becomes more difficult with tail winds since, to maintain the same inertial glidepath, the aircraft path relative to the air mass becomes steeper with even lower trim power.

There are presently no certification criteria for evaluating STOL autoland performance with the steep approaches now possible with MLS guidance. The only available guidelines for certification of autoland systems are those for CTOL jet transports using the conventional Instrument Landing System (ILS) with its fixed glide slope. For these systems, accuracy requirements are specified for the final approach in reference 16 and for touchdown in reference 17. These requirements must be met while considering a prescribed range of wind and turbulence conditions. An objective of this report is to establish a data base to assist in the determination of criteria for STOL aircraft performing steep approaches to landing using MLS guidance.

DESCRIPTION OF SYSTEMS

A description of the aircraft and the avionics hardware is given and then descriptions of the flight-test and simulation facilities are provided. This section concludes with a summary of the navigation, guidance, and control laws. Additional details of these laws are provided in appendix A.

Aircraft and Avionics Systems

The flight tests were conducted with a turboprop-powered de Havilland, DHC-6, Series 100 Twin Otter Aircraft (figs. 1 and 2). The aircraft and power plants were standard with the exception of a wing spoiler installation which was not utilized in the tests reported here. Electromechanical parallel servos were provided for the aerodynamic control surfaces and for the throttle in order to implement the automatic control.

A digital avionics system known as STOLAND (ref. 1) was installed in the aircraft (fig. 3). The computer, which has a 32,000 18-bit word memory, received navigational, aircraft motion, and air data information; processed navigational, guidance, and control functions; and generated signals through appropriate interfaces to the electronic control servos and cockpit displays. Aircraft motions were measured with vertical and directional gyros, rate gyros, and strapdown accelerometers.

Runway Geometry, Navigation, and Radar Tracking Systems

Flight tests were conducted using facilities at the Navy Crows Landing auxiliary landing field. A simulated 610 m STOL runway was painted on the larger runway surface in accordance with guidelines from reference 18. The terminal-area navigation aids available at the site were a Basic Narrow MLS with a horizontal coverage of $\pm 40^\circ$ and a conventional TACAN. Two tracking radar systems provided independent measurements of aircraft position. The STOL runway setting together with the navigation and radar sites are shown in figure 4. The location of the MLS elevation antenna phase center provides a glidepath intercept point (GPIP) of 71.5 m from the runway threshold for a 6.0° approach. Information on the MLS specifications is given in reference 19. Estimates of radar tracking and TACAN accuracy at the Crows Landing installation are presented in reference 20.

Simulation Facilities

The simulation facilities consisted of the airborne computer, a general-purpose digital computer, and a fixed-base cockpit together with the necessary interconnecting equipment. The cockpit was equipped with manual controls and conventional aircraft instruments which were driven by signals from the general-purpose computer. The simulation cockpit also incorporated electronic displays and control panels which were connected to the airborne computer in the same manner as was done in the aircraft.

The general-purpose computer generated the aircraft motions, the navigation signals with appropriate error models, the control surface servo dynamics and servo interlock logic, and the atmospheric disturbances. A unit called an airborne hardware simulator was provided to convert and transmit aircraft motion and navigation signals in aircraft sensor format to the airborne computer, and to return control servo commands from the airborne computer to the general-purpose computer. The system operated in real time and was used for final design and checkout of the airborne software prior to actual flight testing. Additional information on the facilities is provided in reference 1.

Airborne Navigation, Guidance, and Control Laws

All guidance and automatic control functions were implemented in modular form in the onboard digital computer. The modular form facilitated tailoring a function, and the accuracy of the fixed point computational structure, to the requirements of the particular navigation or control mode. An executive program controlled testing for and switching to each particular mode. Only those portions of the system pertinent to the longitudinal results presented in the report will be described. The portions are glidepath track, airspeed control, and flare control laws, together with the generation of the associated filtered navigation signals used for these laws. General descriptions are provided in this section while additional details are given in appendix A.

Navigation– The MLS navigation was utilized during the final approach. Aircraft position was converted from MLS azimuth, elevation, and DME coordinates to runway-referenced rectangular coordinates and to a vertical glidepath error. After conversion, all signals were passed through inertially complemented third-order filters. See appendix A for additional details on the coordinate conversion and filtering.

Final-approach control and filtering– Since the nominal approach speed was selected at 30% above the power-off stall speed to provide an adequate safety margin, the aircraft trim point was on the "front side" of the power-required-versus-speed curve. Hence, final-approach tracking was obtained in the conventional manner with pitch attitude changes controlling outer-loop path and power changes controlling speed. Inner-loop pitch attitude control was obtained with the elevator. Control gains on the final approach were set as high as feasible within stability and control activity limits observed in flight to maintain tight tracking performance in the presence of atmospheric disturbances. In contrast with procedures based on ILS signal capability, path error gains were maintained until the flare-engage altitude was reached (approximately 15 m). The gains could be maintained down to this altitude because the MLS-derived glidepath error signal remained effective.

Airspeed control was achieved with the throttle with additional damping provided by longitudinal acceleration. An inertially complemented filtered airspeed was used as a control signal.

Flare control and filtering– A general description of the flare control is given in this section with more specific details provided in appendix A. The basic control is similar to that developed for CTOL aircraft. However, the susceptibility to atmospheric disturbances and the requirement for a large pitch attitude change for the test aircraft resulted in a touchdown response quite sensitive to off-nominal conditions. Several modifications to reduce this sensitivity were made to the basic control. The basic nominal flare path generated was a conventional exponential function of altitude. A modification was made to the initial part of this path to provide a smooth transition from glidepath tracking conditions to the exponential flare path. The transition reduced the magnitude of transients occurring from off-nominal flare entry conditions. The nominal flare path was tracked by pitch attitude changes commanding the elevator-controlled pitch inner loop. A pitch attitude change of approximately 9° was also needed during the flare. Because of this large change, predictive pitch and elevator commands were added. The commands were applied through the use of an altitude driving function of the form advocated in reference 2. The use of this type of function, rather than a time integration, insured that a selected increment of predictive command would be added over the flare altitude range regardless of the time duration of the flare. Several other functions were added to both the basic closed-loop path and predictive controls to improve touchdown performance. The functions added were based on asymmetrical characteristics of the flare, the need for greater control action during the latter portion of the flare, and wind effects (appendix A).

The altitude and altitude rate signals, used to determine the flare-engage point and to provide subsequent flare guidance, were obtained from the inertially complemented filtering of a radio altimeter signal.

Throttle control during the flare consisted of a constant rate reduction beginning at flare initiation and continuing until idle was reached. The rate was adjusted according to conditions at flare initiation.

SYSTEM PERFORMANCE CRITERIA

A review of performance criteria which are applicable to longitudinal accuracy requirements for automatically controlled aircraft making Category III approaches and landings is provided in this section. These requirements generally have been developed for jet transports using approach geometry corresponding to present day ILS navigation. Hence, some interpretation of the criteria is required for STOL aircraft because of (1) the steeper approach paths made possible by the MLS and (2) the shorter and narrower STOL runways. Ride comfort considerations, which are of particular importance for LWL aircraft, are also discussed.

Final Approach

Tracking performance and ride comfort considerations for the aircraft stabilized on the final approach will be discussed in this section.

Control system tracking performance– Accuracy requirements on the final approach for atuomatically controlled jet

transports landing in Category IIIa conditions are included in reference 16. Two pertinent parts are quoted as follows:

ILS glide slope performance. "From 213 m (700 ft) altitude to the flare engage height, the automatic system should cause the airplane to track the center of the indicated glide slope to within ±35 microamperes (±0.16° for typical ILS sensitivity), 2σ, or ±3.7 m (±12 ft), whichever is larger, without sustained oscillations."

Automatic throttle performance. "The system should automatically adjust throttles to maintain airplane speed to within ±5 knots of stabilized programmed airspeed."

These accuracies on final approach are also intended to be compatible with the touchdown accuracies given in reference 17 which will be discussed subsequently.

In meeting these requirements, effects of disturbances and pertinent parameter variations due to all causes should be considered. One means for complying is to provide probabilities of occurrence for the disturbances and pertinent variations and then to statistically evaluate aircraft performance. In doing this, the accuracy requirement for the automatic-throttle performance is often interpreted in the same way as that for glide slope; that is, 2σ accuracy over the 213-m-to-flare-engage altitude range. These general procedures would be expected to be adapted for STOL aircraft.

The differences in STOL and CTOL approach conditions should not greatly affect the requirements. Note that the descent rate for the two types of aircraft is approximately the same – the STOL forward speed is approximately half that of the jet transport but the glide slope is approximately twice as steep. Thus the time for descent from a given altitude remains approximately the same. However, the use of the broader coverage MLS could justify some reduction in the initial 213-m altitude requirement for a stabilized final-approach track. Note that, while not pertaining specifically to STOL, the use of MLS navigation requires angular specifications in degrees rather than in the ILS microamperes. No definite changes are suggested for the glide slope track or velocity accuracies. However, limited simulation results indicated that ±5 knot velocity excursions for the slower flying STOL aircraft may have a greater impact on STOL than for CTOL touchdown accuracies.

In this report, the same two criteria will be used as part of the evaluation of STOL performance on the final approach. However, statistical averages from flight were calculated over a smaller altitude range (152 to 30.5 m) than that stated in the criterion. Flightpath geometries were generally planned for these tests so that the aircraft would be stabilized on the final-approach path by the 152-m altitude. This lower value was felt justifiable for the more maneuverable STOL aircraft using broader MLS coverage. The averages were terminated at the 30.5-m altitude since the accuracy of the vertical component of the tracking radar deteriorated below this value. In assessing the performance, effects of atmospheric and navigational disturbances were emphasized. Since only a limited range of atmospheric disturbances was encountered during flight, an attempt was made to augment these results through the use of simulation results to determine effects of a wider range of disturbances. This wider range is based on an assumed disturbance model which is described in a subsequent section. Guidelines for the selection of the model were also given in reference 17.

The 2σ accuracy limit stated in the criterion refers, in its broadest sense, to a symmetrical limit about the nominal that should not be exceeded more than 4.5% of the time. No assumption is made regarding the amplitude distribution of the variable. However, in this report, for simplification, and to give more meaningful manipulations of the averages in some cases, the limit was computed as follows. First, a mean and a standard deviation were calculated from the flight data. Then, with the assumption of a gaussian amplitude distribution, a symmetrical increment about the nominal was computed for which $P_e = 4.5\%$. In order to show some amplitude distribution effects, histograms were also presented for several variables.

Ride comfort– Ride comfort performance is of particular importance for an LWL aircraft because of the aircraft's susceptibility to atmospheric turbulence. While the subject has been extensively investigated, no generally accepted standards have been established nor is there a definition of the range of atmospheric disturbances to be considered. However, the analysis in reference 13 was based on ride comfort results from several sources and it will be used as a basis for comparison with the flight results presented here. An objective of the investigation described in reference 13 was to calculate ride comfort ratings for various route segments to obtain an overall rating of trip satisfaction. While aircraft motion was generally the primary factor related to ride comfort, other factors such as temperature, noise, duration of exposure, and seating arrangements were considered. Only the contributions of aircraft motions during the final approach are considered applicable for this report. Note that for a particular comfort rating, the contributions allowed for aircraft motions may be somewhat larger if other factors are not included. As shown in appendix B, with the aircraft on a 6° final approach, vertical acceleration should not exceed 0.06 g (1σ) for a neutral comfort rating of 4.

Touchdown

Geometry relating the final-approach path and the runway with suggested longitudinal touchdown accuracy requirements are given in this section. Criteria presently used for CTOL jet transports are reviewed and suggested changes for a STOLport are presented.

Pertinent geometry for CTOL aircraft is as follows. A navigation requirement for Category III (ref. 21) states that the glidepath shall intersect a point 14 m (50 ft) above the runway threshold within an accuracy of 3 m above the point. The automatic flare for a CTOL aircraft is usually designed to be initiated at a wheel height near this altitude. Hence, when the vertical distance between wheel height and glide slope antenna location is considered, particularly for larger aircraft, the flare mode is engaged before the threshold is reached. Therefore, to accommodate an airborne system switching to a radio altimeter signal at the flare, the terrain prior to the runway which is beneath the flare must be sufficiently level to provide a stabilized radio altimeter signal.

Two requirements for longitudinal landing dispersions are given in reference 17. One requirement is that the longitudinal dispersion should not exceed 457 m (1500 ft) on a 2σ basis but that it need not be symmetrical about a nominal point. For a gaussian distribution, a $+2\sigma$ level of longitudinal dispersion has a probability of being exceeded of 2.3% while a -2σ level has a probability of not being exceeded of 2.3%. Hence, the touchdown range requirement for distributions which may be asymmetrical results in long and short limits with these probabilities. The 2.3% P_e limits on the range and on the touchdown variables to be given subsequently will be referred to as 2σ limits. A further requirement defines a larger region for which a touchdown beyond this region is improbable. The short boundary is 61 m (200 ft) after the threshold and the long boundary is related to the touchdown zone lights and results in a distance of about 762 m (2500 ft) from the threshold for a medium size jet transport. This improbable event for either a short or long boundary has been interpreted in FAA certification performance evaluations as a probability of exceedance of less than $1X10^{-6}$. The British CAA has required $1X10^{-7}$. For a gaussian distribution, the $1X10^{-6}$ exceedance boundaries correspond to a range of $\pm 4.8\sigma$. Note that for a gaussian distribution, the improbable-event requirement is more stringent than the $\pm 2\sigma$ requirement.

For a short STOL runway (610 m), the approach geometry used during flight tests as well as proposed longitudinal touchdown dispersions are shown in figure 5. The threshold crossing height is a lower 7.5-m value as compared with the CTOL one. With flare initiation near a 15-m antenna height, the flare is engaged about 75 m prior to the threshold. Hence, for systems using a radio altimeter for the flare, terrain that provides a stabilized radio altimeter signal for this distance is required. Suggested values, reduced from the CTOL ones, for the $\pm 2\sigma$ and improbable-event dispersion boundaries are also shown in figure 5. The $1X10^{-6}$ long boundary was based on an estimate of aircraft stopping distance whereas the short boundary was located as close to the threshold as was considered feasible.

A comparison of ratios between the CTOL and suggested STOL criteria is useful. The improbable-event dispersion range is approximately twice the $\pm 2\sigma$ range for STOL whereas the ratio is 1.5 for CTOL. Comparing these two values with the gaussian σ ratio for the two dispersion probabilities, 2.4, indicates that the suggested STOL values are a little more compatible with a gaussian distribution. However, the STOL improbable-event criteria are more asymmetrical relative to the GPIP since the STOL value is relatively closer to the short boundary than for CTOL. (The ratio of distance between the GPIP and the short boundary to the total improbable-event boundary range is 0.18 for STOL whereas it is 0.36 for CTOL.)

Several additional touchdown design goals for the test aircraft were included:

$$\theta_{td} \geq -0.5^\circ \ (2\sigma)$$

$$h_{td} \leq -1.8 \text{ mps } (2\sigma)$$

$$V_{c_{td}} \leq 60 \text{ knots}$$

The first two goals satisfy landing gear requirements. The first one requires initial contact on the main wheels to avoid an excessive load on the nose wheel, while the second one limits initial contact load on the main wheels. The last goal provided a touchdown speed approximately 10% above the stall speed.

ATMOSPHERIC DISTURBANCES

Estimates of wind and turbulence encountered in flight are given in this section. Representations of wind shear and turbulence for use in the simulation are also described. Finally, an atmospheric disturbance model is provided in the form of a distribution of wind and turbulence for use with the simulation and for summarizing flight-test results.

Wind and Turbulence Estimates from Flight

Since the LWL test aircraft was quite susceptible to atmospheric disturbances, a knowledge of the levels encountered was important in the assessment of tracking performance. Although the aircraft instrumentation was not specifically designed for wind and turbulence measurements, it was adequate to provide estimates of these disturbances. The measurements were processed as part of a postflight digital data analysis program. The horizontal wind along and perpendicular to the runway was determined by a differential calculation of aircraft ground and airspeed measurements. Although the vertical wind variation is also a significant factor for the aircraft longitudinal response, instrumentation difficulties, particularly in the angle-of-attack measurement, precluded determining this component with sufficient accuracy. For the horizontal wind, aircraft ground speed was estimated

through the use of the tracking radar, whereas airmass velocity relative to the aircraft was estimated through the use of airspeed and airflow direction measurements. Details of the data analysis are given in appendix C. The measured flight results are presented in this section.

The horizontal winds encountered by the aircraft on the glidepath over the altitude range between 152 and 30 m above the runway were summarized for each approach in the form of statistical averages. A mean, representing the average wind, and a standard deviation, representing the turbulence level, were calculated over this range. The values of turbulence should be used with some caution since the instrumentation was not designed for this more precise dynamic requirement. While wind averages for altitudes below 30.5 m including the flare would certainly be pertinent, further accuracy problems in this region made the wind estimates unreliable. Winds in this region were more difficult to measure because of wind shear (boundary-layer effects) as well as measurement inaccuracies associated with increased aircraft motions.

A more complete analysis of the turbulence would include estimates of frequency content and amplitude distribution. While these additional aspects were beyond the scope of the investigation, the following assessment of frequency content can be made. An estimate of the effective measurable bandwidth can be obtained from characteristics of the data-smoothing filter. As described in appendix C, polynomial filtering over 1.5-sec increments of the airborne data was used. This time interval was a compromise between achieving signal bandwidth as high as possible and the necessity for rejecting noise. For an aircraft speed of 70 knots, the filter passes signals with wavelengths of 90 m or greater. For another assessment, spot checks of the wind frequency content were made by calculating the autocorrelation functions of selected wind time histories for the same altitude range from 152.4 to 30.5 m. The autocorrelation function was chosen rather than the power spectrum because the former was felt to allow a more accurate dynamic estimate for the relatively large ratio of wavelength range of interest to total distance involved. The check cases indicated that horizontal gust lengths of the order of 125 to 150 m were typical. By comparison, the average horizontal gust length used in the simulation (appendix C) for this altitude range was somewhat longer (278 m). While not specifically investigated, the frequency characteristics of the flight results were felt to be relatively stationary over the altitude range summarized.

Typical variations with distance along the glidepath, representing the range of disturbances encountered during the flight-test period, are shown in figure 6. Graphic letters, H for head winds and T for tail winds, and solid lines for low winds are used to identify average wind conditions. This symbolism will be utilized to label wind conditions for subsequent path histories of aircraft responses. The winds are shown as a function of radar-measured horizontal distance from the elevation phase center,[1] and the data are terminated at touchdown. The previously selected 152.4- to 30.5-m altitude range used for statistical averages corresponds to a 1427- to 267-m horizontal range on the 6° glide slope. The approaches with head winds show the largest amount of turbulence as well as some decreasing wind shear near the runway.

Mean values of horizontal wind for each approach analyzed are presented in figure 7. Examination of the figure shows that the longitudinal wind components can be combined into three groups – head, low, and tail winds. Statistical averages of wind and turbulence for the three groups are given in table 1. The wind averages for each group represent the mean, μ, and the rms, σ, relative to μ, of the average winds obtained from each approach in the group. The turbulence average, σ_a, represents the rms of the turbulence levels obtained from each approach. The wind standard deviations are a quantitative measure of the variations shown within each wind group in figure 7. An examination of the number of approaches in each group (table 1) indicates that a larger number of head-wind samples would have been desirable for determining statistical averages more accurately. However, the separation of the results into these three groups is felt to provide the best use of the available data. Results from the table indicate that turbulence was higher with the larger wind magnitudes and the largest value occurred with the 13-knot head wind. In subsequent presentations of aircraft performance results, the statistically averaged data will be separated into these three wind groups. Moreover, since there is a preponderance of approaches with tail-wind conditions, a correction to more standard wind distribution conditions will be applied when overall aircraft-response statistical averages are obtained. The correction to be used is based on the wind distribution model which will be described subsequently. Overall averages obtained through use of the model will be called combined averages and the values for the longitudinal component are also shown in table 1.

To help substantiate the accuracy of the onboard wind measurements, the values were compared with two ground sources. One source was located on a mast near the touchdown zone at an altitude of 4.6 m above the runway and was continuously recorded. The other source was used by the control tower and was near the tower at an altitude of about 15 m. This source was generally reported only once during the approach. Averaged samples from the 4.7-m ground mast, which were taken at the time the aircraft passed the 4.7-m altitude (just before touchdown) on each approach, are shown in table 2. A comparison of wind results in tables 1 and 2 shows that the lower altitude ground-measured winds follow the well-known trend of being lower in magnitude than the higher altitude winds. This reduction indicates possible wind shear effects. As previously mentioned, some difficulties were encountered with the onboard wind

[1]The phase center is the location of the electronic origin of the signal transmitted from the antenna.

measurements at the lower altitudes so that it was not considered feasible to compare onboard with ground-measured winds as the aircraft passed the 4.7-m altitude. Although not shown, the tower-reported winds were generally in about the same direction as the mast winds, but were often about 5 knots higher.

To further describe atmospheric conditions during the tests, typical temperature profiles are shown for each of the three wind conditions (fig. 8). Also shown for comparison is the standard temperature variation with the altitude converted to horizontal distance for the nominal 6° glide slope. The slopes of measured temperature with distance are seen to be approximately the same as the standard temperature slope, thus indicating that neutrally stable atmospheric conditions generally prevailed during the tests.

Simulation of Wind and Turbulence

To further delineate effects of atmospheric disturbances on aircraft performance, simulation results using wind and turbulence were utilized. The simulated disturbances selected encompassed a wider range than those encountered in flight in order to allow more direct comparisons with criteria. Because of the previously mentioned problems in estimating the wind-spectrum characteristics from flight measurements, these characteristics were not modeled directly in the simulation. Instead, standardized wind shear and turbulence models were used. For wind shear, both log-linear (ref. 22) and FAA-linear (ref. 17) models were used. For turbulence, a Dryden frequency distribution with altitude-varying parameters (ref. 23) was incorporated. The disturbances are further described in appendix C.

Atmospheric Disturbance Model

An atmospheric wind and turbulence magnitude model based on a range of disturbances similar to those that would be encountered by an operational aircraft is discussed in this section. A more specific description is provided in appendix C. The model was used (1) to adjust statistically averaged responses to reflect a more typical distribution of wind than that actually encountered during flight testing, and (2) to select realistic magnitudes of wind and turbulence for the simulation. The model was based on FAA recommendations for evaluating CTOL aircraft (ref. 17). The wind distribution model covers a range from 25-knot head winds to 10-knot tail winds at the reference altitude of 7.6 m (25 ft) (see appendix C for the probability distribution). For a particular wind magnitude, the model turbulence level (1σ) was 15% of that magnitude. To represent the turbulence in the simulation over the range of atmospheric conditions of interest, the magnitude distribution was simplified as described in appendix C.

MLS NAVIGATION ACCURACY

As part of the assessment of overall aircraft performance, the effects of MLS navigation errors were investigated. The assessment can best be made through the use of simulation results since effects of the MLS errors in flight could not be separated from the other disturbances. As an initial step, the MLS errors will be presented and compared with specifications in this section. To do this, the procedure for processing the errors into a form for comparisons with specifications is first outlined. Then the flight-measured errors are presented and the comparisons made. Finally, the MLS noise model developed from the flight measurements for use in the simulation is described. More specific details of the data analysis and noise model are given in appendix D. The errors presented are based on the signals received by the airborne computer and consequently reflect only the filtering used in the airborne receivers.

Data Reduction Procedure

Estimates of MLS errors are obtained by comparing the MLS-derived position with radar tracking measurements through the use of a postflight digital data reduction system. The resulting unfiltered total MLS error data was further reduced to achieve two purposes. One purpose, which is described in this section, was to reduce the errors to a form that could be compared with MLS specifications. The other purpose, which will be described subsequently, was to obtain a representation of the errors for use with the simulation. To reduce the data to a form for comparison with MLS specifications, the basic data was passed through both a low frequency path-following error (PFE) and a higher frequency control motion noise (CMN) specification filter (refs. 24 and 25). Means and standard deviations of the outputs were obtained. For a particular approach, the PFE could be separated into an average or bias value, plus a low-frequency random component, whereas the CMN contained only a higher frequency random component. Only errors from the elevation and DME signals are presented, since only these functions affect the longitudinal performance.

The total (unfiltered) MLS errors were determined by comparison with the tracking radar. The radar measurements, expressed in rectangular runway coordinates, were filtered (see appendix C), transformed to MLS coordinates (see appendix D) and compared with the signals obtained from the MLS receivers. Note that the resulting difference includes MLS errors due to ground-signal generation, air propagation, and airborne receivers plus any residual errors in the radar measurement. Accuracy problems were encountered with the radar vertical tracking at altitudes less than about 30 m. In this region, ground multipath reflections interfered with the

automatic radar angular tracking and caused a reversion to a lower accuracy manual tracking mode. Hence, elevation errors will not be shown below this altitude (260 m horizontal distance from the elevation antenna on the 6° glide slope).

Flight Results

Typical variations with distance along the glidepath of the elevation and DME errors are shown in figure 9. A typical pair of approaches is given for each of the three basic wind conditions encountered. The wind, of course, has no particular relevance for these results and thus the examples indicate only three pairs of approaches on three different days. No significant variations occurred with distance in the final-approach region shown. A large part of the variation in range is due to changes in bias on different days.

Typical variations in the total (unfiltered) MLS errors as well as the path-following and control motion (filtered) MLS errors are presented in figure 10. The specifications for this system (ref. 19) are also shown. At the time this MLS system was designed, the PFE and CMN specifications were used only for the angular signals. The single DME specification was for the total error. Details of the filter constants and their implementation to obtain the test data are given in appendix D. Also shown in figure 10 is the ILS ICAO specification for low-frequency angular error (ref. 21). Note that the path-following MLS elevation specification for a glide slope of 6° is somewhat more lenient than the ILS value. This difference mainly reflects the relaxation in the MLS specification for a glide slope greater than the approximately 3° CTOL value. Reference to the figure indicates that both elevation and DME errors are well within the specified values for this approach.

Statistical averages for all approaches over the 152.4 to 30.5 m altitude range are presented and compared with specifications in table 3. The procedure for weighting the data and calculating the 2σ levels is outlined in appendix D. Note that the 2σ values of the bias are mainly a consequence of the day-to-day variations. These variations form the major contribution to the PFE. No attempt was made during the tests to adjust the bias of either the ground transmitter or any of the several airborne receivers used. The results show that for the region evaluated, the elevation errors were just within and the DME errors were well within the specified values.

MLS Error Model

In order to provide an assessment of the effects of MLS-error dynamics on the autoland system, a noise error model was developed from the approach flight data in the 152.4- to 30.5-m altitude range for use with the computer simulation. Emphasis was placed on the representation of random noise since bias effects on performance could be determined largely through geometric or other considerations. The noise model was obtained from the total (unfiltered) MLS error with the bias removed rather than from separate PFE and CMN filter components. As long as a reasonable representation of the total noise can be achieved, the proportions of random PFE and CMN in the representation are the same as that which would be estimated directly through the use of the MLS specification filters. The noise characteristics did not show any trend during the flight-test period. Hence, each noise parameter was based on the unweighted mean of the values from all approaches. The form selected for the error model was the output of a first-order filter driven by white noise. The two constants required from the flight data were the output magnitude and time constant of the filter. Procedures and data selection for obtaining these constants are given in appendix D.

Values for the MLS error model are presented in table 4. To show the relationship of the frequency content of the model to the MLS specification format, the ratios of path-following and control motion to total noise, calculated from the matched time constants, are also shown. Selective checks of these ratios for a portion of the flight data were made by filtering the measured error data directly with the path-following and control motion filters and comparing them with the unfiltered values. Although not shown, the calculated ratios were within ±15% of the filter ratios given in the table. The noise magnitudes and time constants shown in table 4 were used in the simulation to evaluate the effects of MLS errors on aircraft tracking performance. These results will be presented in subsequent sections.

SYSTEM PERFORMANCE

Flight-test results are presented and compared with criteria developed from CTOL evaluations described in a previous section. The results are also intended to provide part of a data base needed to facilitate the subsequent establishment of more comprehensive STOL criteria. A complete evaluation of aircraft performance would require consideration of all pertinent effects. However, such a general assessment was beyond the scope of this report. Because of the susceptibility of the LWL aircraft to atmospheric disturbances, emphasis was placed on evaluating these effects. Consideration was also given to the influence of navigation errors on performance. Performance on the final approach and then touchdown for approximately 80 approaches will be shown.

Flight results were augmented when feasible by simulation results to facilitate comparisons with criteria, since they were generally based on aircraft responses to a wider range of conditions than those encountered in flight. Effects of atmospheric disturbances and flight-determined MLS errors on

aircraft performance will be shown through use of the simulation.

Final Approach

Generally, nominal final-approach paths were planned so that the low-frequency modes of the aircraft were stabilized on the 6° glide slope when an altitude of 152 m was reached. This objective was conservatively accomplished by the selection of a glide slope capture altitude of about 300 m with the aircraft in the final-approach configuration and airspeed. However, for various reasons the entry for approximately 40% of the approaches did not allow this condition to be met. For instance, flight patterns were contracted for a number of approaches to concentrate on achieving touchdown data. The result was that statistical averages of low-frequency variables, such as glidepath and airspeed errors, that included the 152 m altitude could be obtained for only the remaining reduced number of approaches.

A final-approach speed of 71 knots was selected for the aircraft at a maximum gross landing weight of 4990 kg (11,000 lb). This selection provided a speed margin of 30% above the stall speed. The same stall margin was maintained as fuel was expended by reducing the approach speed. These speeds resulted in trim on the conventional front side of the power-required-versus-speed curve. The maximum gross weight corresponded to a wing loading of 1250 N/m^2 (26 lb/ft^2).

The flight results for the final approach are shown as typical variations of performance parameters with distance along the glidepath, histograms at selected points on the glidepath, and statistical averages of both of these forms. The averages along the glidepath were obtained for the 152.4- to 30.5-m altitude range. The upper limit was selected from the previously mentioned stabilized tracking considerations. The lower limit was the altitude at which the vertical radar tracking signal began to deteriorate. However, for the primary tracking variables, histograms are given at the lower flare-engage altitude (about 15 m) as well as the 152.4- and 30.5-m altitudes. The results are grouped by the winds encountered, and by a wind-weighted overall combination. While the effect of the mean wind was not significant for aircraft motion variables on the final approach, the turbulence associated with each wind group did allow further delineation of atmospheric effects.

Glidepath system performance– A description is given in this section of glidepath tracking performance. The results evaluated are glidepath tracking error relative to the onboard measured path, the approach plane tracking error useful for obstacle clearance information, control activity, and ride comfort.

Glidepath tracking performance. The performance measure shown was the complementary filtered glidepath error signal. The signal was used for outer-loop path control and is related to the vertical tracking variable for the criterion described in a previous section. Typical variations along the glidepath during each of the three previously described wind conditions are shown in figure 11. The initial transient with the tail-wind data is not significant as far as capture capability is concerned but only reflects the lower capture altitude used for these particular approaches. Histograms of vertical error are shown at the 152.4- and 30.5-m altitudes and at flare initiation in figure 12. Results are given for the three separate as well as the combined wind conditions. The combined results were obtained by combining the separate wind histograms through the use of weighting factors associated with the wind distribution model described in the "Atmospheric Disturbances" section. The mean values and standard deviations for the histogram data are given in table 5. The standard deviation for the combined wind is based on deviations relative to the combined mean. Examination of the histogram shapes indicates that they are close enough to gaussian amplitude distributions so that meaningful comparisons can be made through the use of lumped mean and standard deviation calculations. The flight results show that the excursions are quite small and no significant trend is apparent with either altitude or wind conditions. Altitude differences are minimal principally because constant position error control and filter gains were used in this portion of the final approach. The mean values are also small, thus indicating that control integral terms were adequate to reduce initial transient effects and to compensate for the different winds.

The flight results, averaged over the 152.4- to 30.5-m altitude range, are compared with simulation results and the CTOL criterion in table 6. The flight value represents average deviations relative to zero error and is weighted by the wind distribution model. Separate simulation results for turbulence (based on the atmospheric disturbance model) and MLS noise are shown to assess effects of each disturbance. Effects of the MLS errors are small and reflect mainly the elevation angle component. The result for summed MLS noise and turbulence from the simulation is also shown. Because of the previously mentioned problems with the estimation of turbulence levels from flight results, a direct comparison of flight with simulation results cannot be made. However, both flight and the summed simulation results are seen to be much less than the CTOL requirement.

Aircraft tracking relative to the final-approach plane. Another useful assessment of path tracking performance is the tracking accuracy of the actual aircraft position relative to the inertially fixed final-approach plane. This type of information provides obstacle clearance requirements although the tracking of an automatically controlled aircraft on the last portion of the final approach is sufficiently

accurate so that it is not expected to be a significant factor in this determination. While total excursions for the flight conditions encountered could have been determined directly from the radar tracking data, it was more useful to combine simulation results, which reflected the effect of the atmospheric disturbances model, with the measured navigation error. Hence, total tracking displacement was obtained from a combination of navigation bias error (obtained from flight measurements) and the true vertical dynamic error (obtained from simulation results using the matched MLS noise error and the atmospheric disturbance model). The procedure employed for calculating the total was the same as that used to calculate MLS PFE from elevation bias and random path-following noise (appendix D). Note that the definition of vertical dynamic error is slightly different from the vertical error used in the "Control system tracking performance" section. The former is defined as the true vertical difference between the aircraft position and the biased MLS nominal approach path. The latter is the indicated difference (as measured by the onboard complementary vertical filter) between the aircraft position and a biased nominal approach path. The difference between these two definitions results from the low-frequency MLS elevation path-following noise passed by the onboard filter. The results are listed in table 7 with the elevation bias value calculated from table 3. The resulting total error is quite small.

Control activity. Typical variations along the glidepath as well as statistical averages over the 152.4- to 30.5-m altitude range of elevator position and pitch attitude are shown in figure 13. Pitch attitude is included as a control variable because of its use as a path command control. The command to the elevator-controlled pitch SAS rotates the aircraft to achieve the path change. The results shown are grouped as functions of the flight winds encountered. The mean values represent trim conditions associated with these winds. Note that no significant trim variation with wind occurs for the elevator. The σ_a value for each wind condition is the rms of the standard deviation for the approaches in each group. The effect of the MLS noise is small. Figure 13 also indicates that the greatest control activity occurs during the head winds and is a result of the larger turbulence level encountered. However, this highest activity level is still considered to be relatively small.

Another aspect of control activity is the longitudinal column motion associated with automatic-control systems in which the column is mechanically connected to the elevator, and the automatic control is actuated by a servo attached parallel to the connection. The resulting low-frequency-column motion cues are useful to the pilot for monitoring control system activity but high-frequency activity is annoying. Hence, control noise levels as well as more positive actions can be ascertained. As shown by the table in figure 13, the highest elevator and associated column activity occurred during head-wind conditions. For these conditions, the column activity was σ_a = 4.5 mm (0.2 in.). This value is considered to be relatively small.

Comparisons of flight and simulated pitch attitude variations are made with the ICAO ILS criterion (ref. 21) in table 8. This criterion prescribed a limit on aircraft attitude excursions at the last part of the glidepath (15 m altitude) due to low-frequency beam bends. For each wind condition the flight result, $2\sigma_p$, represents the increment relative to the pitch attitude trim. The trim was obtained from the mean value from each set of approaches for the 152.4- to 30.5-m altitude range. The effects of the MLS errors on aircraft motions are within the ICAO criteria since, even with other factors affecting the flight motions the resulting excursions are less than the criterion. The simulation results using the MLS noise error model were obtained by averaging the aircraft response along the final-approach path over the 152.4- to 30.5-m altitude range. The path average over this altitude range was more expedient to perform with the real time simulation than the ensemble average that would be needed for the 15-m altitude stated in the criterion. However, the result is a conservative estimate for the lower altitude since the elevation errors produce greater attitude errors at the higher altitudes. The response resulting from the noise model is much less than the criterion's prescribed limit.

Ride comfort. Typical final-approach variations and average rms values of vertical acceleration responses are shown in figure 14. Again, the approaches with maximum excursions occurred for the higher turbulence levels associated with the head-wind conditions. While no extensive analysis of the frequency content of the signal was made, spot checks indicated that the principal content was near the aircraft short-period frequency (0.4 Hz). The combined-wind flight-determined acceleration rms average is compared with simulation results and the ride comfort limit for neutral acceptance described in the "System Performance Criteria" section (table 9). The combined-wind flight results and the previously shown larger head-wind results are well below the comfort limit. Simulation results due to 1σ levels of MLS noise and turbulence are also shown. As would be expected, the effect of MLS noise is relatively small in comparison with the turbulence. While not shown in the table, simulation results indicate that the horizontal component of turbulence made a significant contribution to the total vertical acceleration due to turbulence. When applied separately, the horizontal turbulence component caused a vertical acceleration level of about 80% of that resulting from the vertical component. This result indicates the need to consider horizontal turbulence in the vertical control design. Simulation results also show that with the MLS noise level held constant, increasing the turbulence level to a value of 1σ = 2.9 knots (4.9 fps), the aircraft acceleration level would reach the ride comfort limit of 0.06 g. This level corresponds to a 5% probability of exceedance (about 2σ) for the atmospheric model.

Control system modifications to reduce the acceleration levels, even at higher altitudes where more precise glidepath track control is not needed, may be difficult for the LWL aircraft using conventional controls. In addition to difficulties associated with accurate turbulence sensing, the conventional elevator control system must contend with the lag associated with the need to first measure and then pitch the aircraft in order to counteract the gust disturbance.

Airspeed system performance– Performance of the speed control system is given in this section. The flight results presented consist of the airspeed tracking error and engine activity. Airspeed results from flight measurements are augmented with simulation results to facilitate comparisons with the criterion.

Airspeed tracking. Airspeed tracking accuracies are shown for the last part of the final approach in the same manner that was done for glidepath error. First the flight results are presented and compared with the criterion and then simulation results appropriate to disturbances specified by the criterion are shown. The controlled variable is an inertially complemented airspeed (appendix A) and the flight results are presented as variations along the glidepath (fig. 15), histograms (fig. 16), and summary averages (table 10). The previously used pattern is followed with the results given for three wind conditions and a combined form based on the weighting factors from the wind distribution model. As was done for the glidepath error, all approaches for which the aircraft velocity was not quite stabilized at the 152.4-m altitude were omitted from averages which included that altitude. Results from the figures and table indicate that the velocity error is well within the ±5.0-knot criterion for the flight conditions encountered. The nominal approach speed of 30% above stall (about 15 knots in terms of velocity error) provided a sufficient operating margin for the light-to-moderate turbulence conditions encountered. No significant effect of steady wind was present.

The flight results, averaged along the approach path over the 152.4- to 30.5-m altitude range, are further compared with simulation results and the CTOL criterion in table 11. Again, the separately shown MLS and turbulence results from the simulation are given to assess the effects of these disturbances. As would be expected, the contribution of the MLS noise is not significant since the MLS variables are not used directly in the airspeed control. The simulation result for turbulence is based on the atmospheric disturbance model. As previously discussed, the simulation and flight results cannot be directly compared because of accuracy problems encountered with the estimation of turbulence from flight. However, both flight and simulation results are much less than the CTOL limit.

Airspeed control activity. Engine torque measurements were selected to reflect throttle and engine activity levels associated with the airspeed control. Small changes in the variable are approximately proportional to changes in engine power even though small changes in rpm occur with the low-power settings on the approach. For this power range, throttle activity can be estimated from the torque variations by the ratio, 0.043% of full-throttle travel/N•m. Example variations along the glidepath (for the right engine) as well as statistical averages (based on both engines) over the 152.4- to 30.5-m altitude range for the separate wind conditions are shown in figure 17. The increase in mean value with increasing head wind indicates the higher trim setting needed to maintain the flatter aerodynamic descent angle required in increased head winds. The variations are seen to be relatively small in comparison with a nominal take-off torque of about 1900 N•m (1400 ft-lb). Hence, these levels are not believed to have any significant effect on throttle servo requirements or on passenger sound annoyance.

Touchdown

Touchdown performance is assessed in this section first from flight results and then from simulation results. Comparisons are made with applicable criteria and design goals. The basic touchdown performance variables from flight – radar-measured longitudinal distribution, sink-rate, pitch attitude, and airspeed – are presented in the form of histograms (fig. 18) and statistically averaged results (table 12). Results are shown for the three separate and the combined wind conditions. The latter result was obtained through use of the previously described wind distribution model. The boundaries labeled "measured 2σ probability" in the combined histograms are 0.023 P_c values obtained directly from the histograms. Comparisons of the performance obtained from the combined histograms with the statistical design goals are summarized in table 13. Note that small differences exist between the 2σ combined values obtained from the histograms (table 13) and those that would be obtained from the μ and σ combined values given in table 12. These differences are due to nongaussian distribution and round-off effects.

In contrast with the final approach results, aircraft performance at touchdown is sensitive to values of mean wind and turbulence. In head winds, the aircraft tends to land somewhat shorter and harder, and with a more positive pitch attitude. In tail winds, the opposite changes occur with the aircraft floating longer and landing softer, and with a lower, marginally positive pitch attitude. The histogram of touchdown position indicates that although a number of the head-wind landings were short of the GPIP, they were still within the improbable-event boundary of -56 m. Airspeed at touchdown does not show any appreciable trend with wind. The wind affects touchdown distance because of the resulting changes in ground speed. The effect is more pronounced for slower flying STOL than CTOL aircraft since the same wind

speed differences result in relatively larger changes in ground speed. The use of greater power (slower throttle retard) would have been desirable for the head-wind conditions encountered.

The 2σ touchdown design goals (described in the "System Performance Criteria" section) were met for the flight conditions encountered (table 13). The longitudinal dispersion was within the goal whereas the goals for sink rate and pitch attitude were only marginally achieved. The goal of a touchdown velocity at least 10% higher than stall (approximately 60 knots) was also attained (table 12 and fig. 18(b)).

Further insight into the trends with wind can be obtained from the comparison of flight and simulation results shown in figure 19. To estimate the sensitivity of touchdown results to wind structure, simulation results were generated using the following sets of winds: (1) a runway-aligned wind without a cross-wind component or wind shear. (2) A runway-aligned wind plus a cross-wind component obtained by interpolation of the flight-measured cross winds. (3) A runway-aligned wind with the same cross-wind component plus the log-linear wind shear profile described in appendix C. To be comparable with flight results, the simulated wind shear results in this figure were referenced to an average value over the same 152.4- to 30.5-m altitude range that was used for the flight winds. An examination of figure 19 shows relatively large changes between the low- and head-wind conditions. Simulation results show that both the cross-wind and wind shear effects may contribute to a large portion of this shift. The decrease in longitudinal touchdown location with the cross wind may be due to the increase in aircraft drag. Even though the aircraft is aligned with the runway during flare by a "forward slip" maneuver, the lateral-directional control action and roll attitude result in higher drag with cross winds. A head-wind shear will tend to reduce the longitudinal touchdown point primarily because of a reduction in airspeed and a corresponding reduction in lift. While the accuracy of the flight wind estimate near flare deteriorated from that at higher altitudes, the data suggest (fig. 6) that a significant amount of wind shear was present with the head winds. In addition, an increased pitch attitude with head winds at touchdown is indicative of control response to an altitude loss due to wind shear during the flare (table 12). For the tail-wind condition, the best agreement with flight results occurred for the simulation case without wind shear. (The amount of cross wind was too small to be significant.) While simulation results indicate that a tail-wind shear would have an appreciable effect on longitudinal touchdown, the flight wind estimate did not indicate any significant amount of shear present.

Further simulation results on the effects of wind shear for the entire wind range of interest, are shown in figure 20. The two wind shear shapes are described in appendix C. The log-linear wind shear is a steeper gradient near the ground and it has the greatest effect on the aircraft landing. For this wind shear, the aircraft has an increased tendency to land short in head winds and long in tail winds. The effect of wind shear in tail winds is to increase aircraft energy. This increase causes the aircraft to float and results in difficulty in achieving positive pitch altitude and reduced airspeed.

Comparisons of the simulation results (fig. 20) and the flight results (table 13) with the criteria indicate that, for a broader range of winds and wind shears (and probable increased turbulence levels) from those encountered in flight, some difficulty may be encountered in achieving all of the design goals. This conclusion follows even after allowing for the lower probability of encountering the more extreme winds. Hence, modifications were considered for improving performance for the more extreme head- and tail-wind conditions. While not shown, simulation results indicate that the behavior in head-wind shear could be improved by the addition of a closed-loop airspeed control with a commanded decreased airspeed with altitude during flare. This addition would result in an increase in aircraft power to counteract the energy loss due to the wind shear. Simulation results indicated that the system response would be sufficiently fast to control the low-frequency wind shear changes. However, the response was not sufficiently fast to be effective for higher frequency wind turbulence. An average improvement could also be achieved by increasing the approach speed as a function of head wind but this change would not be selective with varying amounts of wind shear.

To improve touchdown attitude in tail winds, closed-loop throttle control would not help. Since the aircraft power is already at a minimum throttle setting for tail winds, a further reduction in aircraft energy cannot be achieved in this manner. Four alternatives are possible but each one would violate a design goal or require an aircraft redesign. (1) A longer landing goal would be beyond the desired touchdown zone. (2) A decreased approach speed would violate the requirement of an approach speed at least 30% above the stall. (3) A two-segment approach path with a transition to a final 3° glide slope would, of course, be a departure from the desired approach geometry. (4) An aircraft could be redesigned to allow a negative pitch attitude at touchdown, or to achieve a less negative pitch attitude on the final approach. Simulation results indicate that with a flare control modification the longitudinal touchdown in the presence of the 10-knot log-linear tail-wind shear could be reduced about 50 m without an excessive sink rate if a 3° negative pitch attitude was acceptable.

A comparison was also made of the longitudinal touchdown range dispersion from these flight tests with two other flight evaluations using the Twin Otter aircraft (table 14). As stated in the Background and History section, these results were obtained from tests utilizing manual tracking on a steep final approach to a decision height followed by a manual touchdown on a STOL runway. While the results are not strictly comparable because of different test objectives and environmental conditions, it is of interest to note the similarity in the touchdown accuracies achieved.

CONCLUDING REMARKS

A series of flight tests were conducted to evaluate a digital autoland system for an LWL aircraft capable of flying steep (6°) approaches to a STOL runway. Results describing longitudinal performance on the final approach and touchdown together with comparisons with pertinent criteria were given. In order to provide a better foundation for future FAA requirements, results were augmented to encompass a wider range of disturbances from those encountered in flight, through the use of a simulation. The simulation included a representation of the controlled aircraft with atmospheric and MLS disturbance models.

Acceptable performance was achieved by the autoland system at touchdown for the flight conditions encountered. Longitudinal range dispersions were within the 2σ touchdown design goals but sink rate and pitch attitude were marginally close to the 2σ design goals. For conditions associated with the maximum head winds encountered, touchdowns were shorter and harder than for no wind. For large tail winds, touchdowns were longer with lower pitch attitude. Simulation results suggest that difficulties may occur in achieving all of the design goals in the presence of more extreme wind and associated wind shear and turbulence conditions than those encountered in flight. Suggestions were made to improve performance under these more extreme conditions.

On final approach, the vertical path and airspeed tracking performance and ride comfort response were satisfactory for the flight conditions encountered. Simulation results indicated that tracking performance would also be well within limits for the range of atmospheric conditions expected. These results further showed that the aircraft-motion portion of ride comfort goals would remain within a neutrally comfortable boundary for turbulence levels up to a 5% probability of exceedence.

A final-approach command speed of 1.3 times stall speed provided an adequate margin for the turbulence conditions encountered and resulted in an adequate stall-speed margin at touchdown. However, a decreased value of approach speed prior to flare entry for maximum tail winds would have reduced the tendency to land long with a low pitch attitude.

The Basic Narrow MLS provided sufficiently accurate signals for automatic final-approach tracking down to the flare initiation altitude of 15 m above the runway.

Estimates of atmospheric conditions are essential for the evaluation of autoland performance for LWL STOL aircraft because of the sensititivy of the aircraft to these conditions.

Ames Research Center
National Aeronautics and Space Administration
Moffett Field, California 94035, November 18, 1982

APPENDIX A

NAVIGATION, GUIDANCE, AND CONTROL LAWS

Software for generating the automatic-control laws and signals to the cockpit displays was implemented in modular form in the onboard digital computer. An executive routine monitored and controlled the testing and flow of the modular routines to follow a selected operational flight sequence. This modular approach enabled programming the various functions so that efficiency in the fixed-point computations could be maximized for each functional requirement. Most automatic control functions were calculated at a 20 Hz rate. Generally, dynamic functions were formed in a manner similar to that used for continuous systems. First-order digital dynamic elements were cascaded to form higher order ones. A complete system of automatic controls and displays were developed for terminal-area use and a summary of the capabilities of the system is given in reference 26. A number of changes were subsequently made in the system (principally software) during the flight-test development process which included a conversion to MLS navigation. Only portions that are pertinent to the present report are described; that is, the automatic systems which generate the longitudinal final-approach tracking and flare functions. Control is switched and reinitialized from the final-approach tracking to the flare mode so that each one will be discussed separately. For clarity, initialization and trim functions are omitted and only the guidance, control, and filtering equations are described. For each mode, the control laws are described first and then the filter configurations for pertinent variables are given.

Final Approach

Since the aircraft operated on the conventional front side of the power-required-versus-speed curve, path control was provided by pitch while speed control was obtained by throttle changes. Simplified block diagrams of path and speed control laws are shown in figure A1. System constants for these diagrams are included in table A1. A conventional form of outer-loop path and inner-loop pitch attitude control was used. The control gains shown in the table were the maximum feasible in order to achieve good tracking performance during the last portion of the final approach. These maximum values were limited by stability considerations and control activity observed during preliminary flight tests. To accommodate initial portions of approaches starting farther from the runway, outer-loop gain reductions as a function of distance from the runway should be used. For these distances, the reduction will allow decreased aircraft motion activity at the expense of lower path tracking accuracy since requirements for the latter quantity become less stringent. A block diagram of the glidepath error complementary filter is shown in figure A2(a). Inputs to the third-order filter are glidepath error, calculated from the MLS coordinates, complemented with vertical acceleration. The transformation from the MLS coordinates to runway-oriented rectangular coordinates and the glidepath error calculation are described subsequently. A third-order rather than a second-order filter was chosen so that the added $K_{\Delta}\ddot{h}$ feedback loop would compensate for any bias in the acceleration measurement. Relative magnitudes of the complementary filter feedback gains were selected to obtain a triple pole $(s + \omega)^3$ form for the denominator of the transfer function. The glidepath error filter frequency was increased with decreased filtered longitudinal distance from the runway so that the maximum frequency was used only during the final portion of the approach (table A1).

The airspeed control is shown in figure A1(b) together with pertinent constants listed in table A1. The basic control law, $F_V(s)$, employs a filtered error relative to the reference airspeed, V_{ref}, for the proportional term as well as an unfiltered error for the integral term. The use of the unfiltered error avoids introducing possible low-frequency (bias) errors from the filter into the integration with the fixed-point computation. The horizontal acceleration feedback provides the basic damping for the system. Note that when the sum of the throttle command, δ_{TC}, and the integrated throttle rate feedback signal is combined with the hardware integration, a first-order lag between the throttle command and throttle position is formed. The second-order complementary filter for the airspeed control signal is shown in figure A2(b).

Flare

The basic flare control is similar to that developed for CTOL aircraft (e.g., ref. 27). Linear combinations of filtered altitude and altitude rate signals obtained from the radio altimeter were used to determine the flare initiation altitude and subsequent closed-loop path guidance signals. The signals provided a flare with a nominal exponential altitude variation. A feed-forward (predictive) pitch command to the SAS was used to rotate the aircraft to the desired touchdown pitch attitude and to produce the basic flare path trajectory. Because of the large command required, a predictive elevator command was added. The path guidance signal provided closed-loop corrective path signals to the pitch command. Airspeed reduction was accomplished open-loop by a constant-rate throttle position reduction to flight-idle and

the decrease in the aircraft descent angle. Because of the susceptibility of the LWL aircraft to turbulence and the large pitch rotation required during flare, several modifications to this basic control were added. These modifications reflect the asymmetrical nature of the flare as well as the desire to keep the gains as high as possible, particularly in the latter part of the flare.

Flare initiation– The flare was initiated when the following equation was satisfied:

$$-\hat{h}_{rw} - K_{fdh}\dot{\hat{h}}_{rw} + h_{fo} + K_{fv}[1 - (\hat{V}_c/V_G)_{ul}] \geq 0 \quad \text{(A1)}$$

The equation is shown by the flare initiation line in sketch (A1) which depicts the flare characteristics. Values of the constants are given in table A2. The slope of the initiation line was determined by the gain, K_{fdh}. The right-hand term in the equation was added to shift the initiation line to a higher altitude in the presence of tail winds. This higher initiation altitude was needed to achieve a more positive pitch attitude at touchdown for this wind direction.

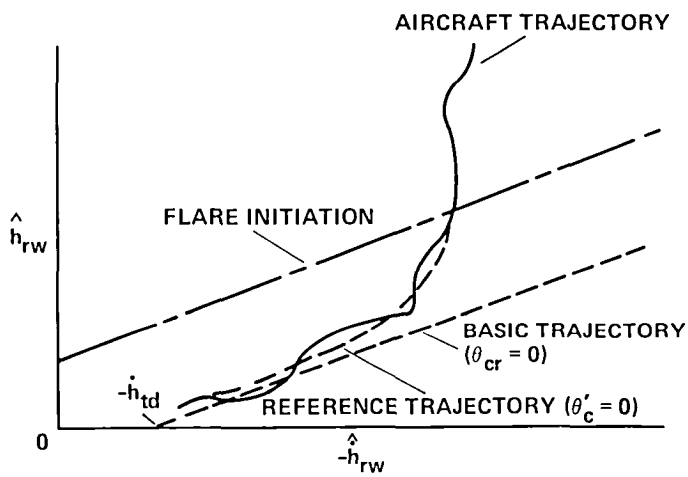

Sketch A1.– Example aircraft tracking of closed-loop flare control.

At flare initiation, several quantities were calculated and stored for subsequent use in flare guidance. These quantities are also given in table A2. The quantities include the limited velocity ratios $(\hat{V}_{co}/V_{Go})_{ul}$ and $(\hat{V}_{co}/V_{Go})_{ll}$ which vary from a unity limit for either tail or head winds, respectively. The subscript o indicates a value determined at flare initiation. These wind-limited functions allow modifications to flare gains in order to account for asymmetrical effects of wind variations on touchdown variables. Another quantity used during flare guidance, ΔV_O, is a velocity increment calculated from a base value dependent on aircraft weight. It provides a basic predictive command to the throttle and a secondary one to the elevator.

Flare guidance– A block diagram of the flare system is shown in figure A3 and the system constants are provided in table A3. The action of the closed-loop portion of the flare control law is shown in sketch A1.

Flare-initiation parameters were selected so that initiation occurred at a differential altitude above the line depicting the basic flare trajectory (sketch A1). The basic closed-loop command signal, θ_{cr}, was calculated from a linear combination of altitude and altitude rate (fig. A3(a)). Perfect tracking of this signal ($\theta_{cr} = 0$) would result in an exponential variation of altitude with time. The altitude differential between the initiation line and the basic trajectory allowed the aircraft to make a transition from the glidepath track to the flare. However, in order to avoid an initial large closed-loop command due to this altitude differential which could cause undesirable transient motions, an incremental quantity which biased the initial command signal to zero was added. The bias was decreased exponentially with time and added to the basic command to form a reference flare command, θ'_c, as shown by the T_c loop in figure A3(a). (The line, IC_O, pointing to the first-order dynamic element indicates the initial condition set at flare initiation.) Thus, the reference command was zero at flare initiation and blended to the basic command during the flare. Perfect tracking of the reference command ($\theta'_c = 0$) would result in a trajectory of the form shown in sketch A1. The use of the reference command in place of the basic command allowed a faster increase (smaller value of the time constant, T_g, in figure A3(c)) of the closed-loop flare gain, $K_1(t,\theta'_c)$, at the start of the flare without inducing a transient.

Three further modifications were made to the closed-loop control law (fig. A3):

1. Effects of wind on the inertial descent rate at flare initiation were accounted for by changes in the slope of the basic closed-loop line and to the closed-loop gain. The no-wind basic slope, K_{hdf}, was multiplied by the limited velocity ratio, $(\hat{V}_{co}/V_{Go})_{ll}$, (fig. A3(a)) and this limit restricted the change to head-wind conditions. As was previously discussed, the needed increase in altitude separation between the flare initiation and the nominal closed-loop (θ_{cr}) lines for tail winds was obtained by increasing the flare-initiation altitude (last term in equation (A1)). For the closed-loop gain, $K_1(t,\theta'_c)$ change, the inverse of the same factor (but unlimited) was used to multiply the no-wind constant, K_4, (fig. A3(c)).

2. The closed-loop gain, $K_1(t,\theta'_c)$ was increased when the aircraft was below a selected low altitude, h_i, and was also below the reference flare trajectory, $\theta'_c > 0$. This change was made to counteract the increased probability of a hard landing under these conditions. The increase was implemented by adding an incremental gain function, $F_g(h,\theta'_c)$ in figure A3(c), defined by the following equation.

$$F_g(h,\theta'_c) = 0 \quad \text{for} \quad \hat{h}_{rw} \geq h_i \text{ or } \theta'_c < 0$$

$$F_g(h,\theta'_c) = K_{ih}(1 - \hat{h}_{rw}/h_i) \quad \text{for} \quad \hat{h}_{rw} < h_i \text{ and } \theta'_c > 0 \tag{A2}$$

3. The initial exponential increase of the closed-loop gain (fig. A3(c)) determined by the lag term, T_g, was delayed up to 1.5 sec if the aircraft was above the closed-loop command line, $\theta'_c < 0$. This delay prevented premature pitch-down action by the closed-loop control. The function is designated by "Delay ($\theta'_c < 0$)" in figure A3(c).

The predictive function, θ_p, supplemented by an elevator predictive function, δ_{ep}, provided a command to rotate the aircraft through the large pitch attitude change to a positive attitude at touchdown (fig. A3(a) and (b)). Because of the short flare time, the predictive pitch command was augmented by a predictive elevator command. The predictive terms were applied through the use of a step function whose magnitude was dependent on the pitch attitude change, $\theta^c_{TD} - \theta_O$, needed during the flare (fig. A3(b)). The function was applied through the use of the faster acting first-order lags, $T_{\theta p}$ and T_{ep}, and by multiplication of the slower acting altitude-driving function, $1 - (\hat{h}_{rw}/h_O)$. The use of an altitude rather than a time integration function insured that a selected amount of predictive command would be applied in the flare regardless of the time elapsed. While the commands were basically open-loop terms, they were modified to the extent feasible to account for off-nominal conditions. One modification was to apply both predictive terms through the use of a "lagged" altitude-driving function which increased more slowly than the actual one, $F_h(\theta'_c)$. The altitude change was lagged only when the aircraft was above a biased increment above the closed-loop line ($\theta'_c \leq -\theta'_{cb}$). This lag retarded action of the pitch-up predictive terms so that the need for counteracting closed-loop pitch-down action was reduced. The lag was obtained through use of the following gain reduction function:

$$F_h(\theta'_c) = 1 + K_{g\theta}(\theta'_c + \theta'_{cb}) \quad \text{for} \quad \theta'_c < -\theta'_{cb}$$

$$F_h(\theta'_c) = 1 \quad \text{for} \quad \theta'_c \geq -\theta'_{cb} \tag{A3}$$

Values of the constants $K_{g\theta}$ and θ'_{cb} are listed in table A3. When $\theta'_c < -\theta'_{cb}$, the gain $F_h(\theta'_c)$ is less than one and thus retards the rate of increase of the altitude-driving function. The resulting lagged function was rate-limited to positive rates only (fig. A3(b)) to prevent a reversal of the pitch-up action of the predictive terms.

Two modifications which provided airspeed corrections to the elevator prediction were made (fig. A3). A step input, dependent on the velocity increment, ΔV_O, was applied at flare initiation through the gain, K_{evO}. A second term provided additional elevator prediction to compensate for the aircraft velocity decrease during the flare and was applied through the gain, K_{ev}.

In the pitch SAS, pitch-attitude and pitch-rate feedback gains were increased from those used during glidepath track. These changes provided tighter tracking of the pitch commands at the expense of some increase in control activity. However, this increase was not considered significant during the flare. To further tighten the feedback response during the flare, vertical acceleration feedback was added through the gain, K_{a_z}.

The complementary filter for the radio altimeter signal used during the flare is shown in figure A2(c). The relative feedback gains had the same ratio as those used for the glidepath error filter in order to form a triple pole. A fixed filter frequency was selected for the flare mode (table A1). The radio altimeter signal to the filter was biased to give a value relative to the main wheels.

An open-loop throttle rate command was used for power control during the flare. A constant throttle retard rate, starting at flare initiation, reduced the throttle position to flight-idle. As shown in figure A3(c), the basic retard rate was adjusted for off-nominal approach speeds, ΔV_O, and sink-rates, $\dot{h}_B - \dot{h}_O$, which were determined at flare initiation. After the flight tests a closed-loop airspeed control with a decreasing speed command during the flare was briefly investigated through use of the simulation. Preliminary results indicated that the closed-loop bandwidth was not fast enough to be effective in correcting most disturbances during the 5- to 6-sec flare interval. However, for low-frequency wind shear variations such as the log-linear shape (appendix C), some improvement was obtained. Hence, as discussed in the "System Performance" section, it is felt that a closed-loop throttle control during the flare should be considered for future systems for this type of aircraft.

Aircraft Position from MLS Coordinates

The airborne equations used for two calculations of aircraft position from MLS coordinates are given in this section. The first calculation is the transformation from MLS coordinates to runway-referenced rectangular coordinates when the aircraft position is within both elevation and azimuth angle coverage. The second one is the calculation of glidepath error from rectangular coordinates when the aircraft is on the final approach.

Aircraft position in rectangular coordinates– The coordinate systems used in the transformation from MLS to rectangular coordinates are shown in figure A4. The MLS angular ground signals were generated in planar-azimuth and conical-elevation form. Consequently, no exact closed-form

equations could be developed for the transformation to rectangular coordinates. The following approximate equations were employed:

$$x = x_{az} - R' \cos \psi_n \tag{A4}$$

$$y = -R' \sin \psi_n \tag{A5}$$

$$z = z_{el} - [(\hat{x} - x_{el})^2 + (\hat{y} - y_{el})^2]^{1/2} \tan \theta_n \tag{A6}$$

$$R' = [R^2 - (z - z_{az})^2]^{1/2} \tag{A7}$$

where R, θ_n, and ψ_n are the MLS navigation range and elevation and azimuth angle measurements of aircraft position and $\hat{x}$, $\hat{y}$, and $\hat{z}$ are complementary filtered values of x, y, and z. An approximation was necessary to calculate R' since z could not be directly calculated from MLS coordinates because of the previously mentioned planar-conical geometry problem. The value of z obtained from the previous computation cycle was selected for the calculation. The approximation resulted in only small errors within the MLS coverage region for which it was needed.

Complementary filtering of the same third-order form used for the glidepath track filter was employed for the rectangular coordinates. The filter frequencies for the x-y coordinates were functions of the signal source, and distance and bearing angle from the transmitter. For the final approach, a separate lateral tracking filter was used which provided the increased accuracy needed during final approach tracking. Within 2.8 km of the MLS elevation angle transmitter on the final approach, which includes the region of interest for this report, both the x and the y lateral-tracking filters were at their maximum frequencies of 0.15 and 0.2 rad/sec, respectively.

Glidepath error– The glidepath error, Δh, was calculated from the following equation:

$$\Delta h = -(z - z_{el}) - (\hat{x} - x_{el}) \tan \gamma_{ref} \tag{A8}$$

where γ_{ref} is the planar glide slope reference angle.

Note that this procedure for calculating Δh accounts for the distortion of the conical elevation angle measurement from the desired planar value. (This distortion becomes significant only at low altitudes.) Also note that the use of the same parameter, $\hat{x}$, in equations (A6) and (A8) largely cancels any errors in $\hat{x}$, due to measurement or a computation cycle delay, for the Δh calculation.

APPENDIX B

CALCULATION OF RIDE COMFORT ACCELERATION LIMIT

The analysis described in reference 13 was used to calculate a neutrally acceptable comfort limit due to aircraft motion on the final approach. While the analysis included a broader range of contributions to ride comfort, only those portions dependent on aircraft motions (accelerations and descent rate) were considered for this report. For an aircraft on a 6° final approach with a 71 knot airspeed, the comfort rating as a function of vertical and lateral accelerations was calculated by the following equation.

$$C = 2.7 + 18.9\,\sigma_{a,v} + 12.1\,\sigma_{a,t} \qquad \text{for} \quad \sigma_{a,v} \geqslant 1.6\,\sigma_{a,t} \tag{B1}$$

where C is the comfort rating with scale from 2 (comfortable) to 7 (very uncomfortable), $\sigma_{a,v}$ is the vertical acceleration level, g, and $\sigma_{a,t}$ is the lateral acceleration level, g.

Flight results for this aircraft indicate that lateral acceleration was approximately related to vertical acceleration by the ratio

$$\sigma_{a,t} \approx \sigma_{a,v}/4.5$$

Upon substituting the value of $\sigma_{a,t}$ into equation (B1), the expression for the comfort rating becomes

$$C = 2.7 + 21.6\,\sigma_{a,v} \tag{B2}$$

Note that the vertical acceleration term in equation (B1) is the predominant one. Hence, only an approximate relation for lateral acceleration is needed when assessing the impact of vertical acceleration on ride comfort. A neutral comfort rating of 4 was selected as the reference condition. Substituting this value into equation (B2) results in a vertical acceleration limit of 0.06 g. Note that this limit would be smaller if other comfort factors for a particular flight scenario were included in the comfort rating.

APPENDIX C

ATMOSPHERIC DISTURBANCES

This section provides an outline of the procedure for estimating wind variations from flight-test measurements, an atmospheric model for interpreting flight and simulation results, equations used for simulating wind and turbulence, and pertinent equations needed for the statistical analysis of the flight data.

Wind Determination from Flight Results

Horizontal-wind estimates were made through the use of a postflight digital data analysis system. A set of equations was developed which combined onboard and tracking radar measurements. Although the instrumentation was not designed for dynamic wind estimation, it was considered adequate when used with postflight data smoothing to obtain estimates of the horizontal-wind variations. The wind velocity relative to local inertial space was obtained by first resolving the aircraft air velocity at the air data boom. The boom contained the angle of attack and sideslip vanes as well as the pitot static probe. Then the velocity at the boom, relative to local inertial space, was computed and subtracted from the air velocity to obtain the wind estimate.

The data were processed postflight through a digital computer. Before applying the wind equations, all measured data were first processed by a wild-point filtering routine, and then by data-smoothing (filtering) algorithms. The wild-point filter detected and replaced large data errors through the use of a least squares first-order data extrapolation combined with an expanding error tolerance test. After substituting interpolated values for wild points in the data, smoothing was performed with a moving least squares second-order polynomial curve fit. A 1.5-sec smoothing interval was selected for all variables except the radar-measured aircraft position. Although the position radar variations were relatively low frequency, particular care was needed since differentiation of the smoothed position data was necessary to obtain velocities. The procedure used for the radar measurement was to apply the smoothing algorithm two consecutive times with a 3.0-sec interval. This two-pass technique had the advantage of improved smoothing of the data with less decrease in the digital filter bandwidth than would occur by the use of a single pass and an increase in the smoothing interval.

Atmospheric Disturbance Model

The atmospheric model presented prescribes a probability distribution of wind and turbulence magnitudes which the aircraft would expect to encounter in operational use. The model was employed to adjust statistically averaged flight-test results to reflect the more typical wind conditions represented by the model and to select the wind range and turbulence magnitude used in the simulation. The model satisfies guidelines given in reference 17 for the range of atmospheric disturbances to be considered in determining the compliance of aircraft-system touchdown performance with FAA criteria. These disturbances are defined at a reference altitude of 7.6 m (25 ft). Altitude variations from this reference are described in the next section. To evaluate longitudinal aircraft-response results, only the longitudinal components (runway direction) of wind and turbulence are needed.

The wind distribution model is shown as a cumulative probability distribution in figure C1. In the determination of the model, a 1% probability of exceedance for 25-knot head and 10-knot tail winds was assumed with a relative distribution of 70% head to 30% tail winds. This ratio has been used in CTOL certification work. To interpolate between these three points on the probability curve, a gaussian distribution shape in each wind direction (straight lines on the cumulative probability plot, fig. C1) was used. Note that the interpolation results in a small discontinuity in probability density (slope of the cumulative probability) at zero wind. However, smoothing the discontinuity would not make a significant difference in the applications of the model, such as in the numerical integration procedure described subsequently in this section.

The characteristics of model horizontal-turbulence amplitude were determined from the longitudinal-wind model. One justification for considering only the longitudinal component rather than the total wind value is that the longitudinal is the predominant direction. For a particular longitudinal-wind magnitude, the rms level of the longitudinal component of horizontal turbulence was assumed to be 15% of this magnitude (ref. 17). For this study, the turbulence magnitude distribution was further assumed to be gaussian. Note also that with the assumption of horizontal isotropy, the level of turbulence in the lateral direction is also defined. This relation, together with the probability distribution of the longitudinal wind, determined the probability distribution of the horizontal-turbulence level.

Simulation of Atmospheric Disturbances

The equations for representing wind shear and turbulence in the simulation are described in this section.

Two wind shear shapes were simulated. A constant gradient wind shear, called the FAA wind shear (ref. 17), is given by the following equation:

$$V_w = 1.6\,V_r \quad \text{for} \quad h_{cg} > 61 \text{ m}$$
$$V_w = V_r[1 + 0.01312(h_{cg} - h_{\text{ref}})] \quad \text{for} \quad h_{cg} \leqslant 61 \text{ m} \tag{C1}$$

The log-linear wind shear, given in a British Air Registration Board document (ref. 22), is defined by the equation

$$V_w = V_r(0.4512\,\text{Log}_{10}(h_{cg}) + 0.602) \tag{C2}$$

Altitude of the aircraft *cg* in the equations is expressed in meters above the runway with the wind reference velocity, V_r, defined at h_{ref} = 7.6 m (25 ft). The gradient for the log-linear wind shear is progressively steeper at lower altitudes (a boundary-layer shape) and, for the same reference velocity, exceeds that of the FAA wind shear at altitudes below 15 m.

The form of the turbulence representation described in reference 23 was used for the simulation. The turbulence magnitude, based on a gaussian distribution, was adjusted (as described subsequently) from that used in reference 23. The wavelength characteristics are consistent with the Dryden turbulence representation. The turbulence magnitude and wavelength parameters are functions of altitude with the horizontal turbulence magnitude constant below a 30.5-m altitude and decreasing at higher altitudes.

The use of the turbulence magnitude distribution over the entire range of atmospheric conditions of interest as defined by the atmospheric model would require the generation of ensemble averages with the simulation. To simplify the simulation procedure, we represented the turbulence over this range of winds by a single gaussian distribution. Since the overall distribution of turbulence as defined by the model was not in this form (because of the slightly nongaussian distribution of the winds used in the model) an approximation was required. For this report, the turbulence representation was only used to generate statistical aircraft-response results on the final approach up to the 95.5% probability range for comparison with criteria. An examination of the cumulative probability distribution of the model turbulence magnitude indicated that for the range of interest the distribution was reasonably close to one based on a gaussian distribution of velocities. A conservative estimate of the magnitude of the distribution was obtained by matching the 2σ level of the gaussian distribution to the 4.5% P_e model distribution level of 2.9 knots. This matching resulted in turbulance with a gaussian distribution and a 2σ magnitude of 2.9 knots at the 7.6-m reference altitude.

Statistical averages of aircraft performance parameters on the final approach were obtained from the simulation over the same (152.4 to 30.5 m) altitude range used for flight data. For this altitude range, average values of horizontal (h) and vertical (w) components of pertinent turbulence parameters are:

Magnitude:
- σ_h = 1.42 knots
- σ_w = 0.74 knots

Scale length:
- L_h = 278 m
- L_w = 91 m

Determination of Statistically Averaged Flight Performance

Equations for obtaining overall statistically averaged flight performance (means and standard deviations) that are based on the wind distribution model (fig. C1) are given in this section. Summarized results using the model are considered more representative than those resulting from the wind distribution actually encountered because of the predominance of tail winds during the flight tests.

The equations presented are intended to provide statistically averaged flight performance results which would be obtained if the aircraft was disturbed by winds resulting from the model probability distribution rather than by the distribution actually encountered in flight. Only the portion of the wind model distribution covering the flight-test range of winds was used. The basic equations for the statistical averages are presented first and then an outline of the numerical procedure used to evaluate them is given. The basic equations are:

Mean:

$$E[x] = \mu_x = \int_{w_{\min}}^{w_{\max}} (\bar{x}|w)p(w)\mathrm{d}w \tag{C3}$$

$$E[(x - \mu_x)^2] = \sigma_x^2 = \int_{w_{\min}}^{w_{\max}} \overline{[(x - \mu_x)^2|w]}\,p(w)\mathrm{d}w \tag{C4}$$

where

w	wind in the runway direction
x	aircraft-response random variable whose statistics are a function of wind
$E[\ ]$	expected value of a random variable
$x\|w$	mean value of x for a given wind magnitude
$\overline{(x - \mu_x)^2\|w}$	mean square value of x for a given wind magnitude

$p(w)$	probability density of the wind defined by the atmospheric model (fig. C1) but normalized to the integration limits
$w(\min)$	largest head wind encountered in flight
$w(\max)$	largest tail wind encountered in flight

The evaluation of equations (C3) and (C4) depends first on determining the mean and mean square of the aircraft response as a function of wind, $\bar{x}|w$ and $\overline{(x-\mu_x)^2}|w$, from the flight measurements. The best procedure for evaluating these functions depends somewhat on the distribution of the wind actually encountered in flight. For a "grouped" form of wind distribution, the functions can be evaluated by separating the data into wind groups, evaluating the statistical averages within each group, and interpolating to obtain values between the groups. The procedure is illustrated for $\bar{x}|w$ in sketch (C1).

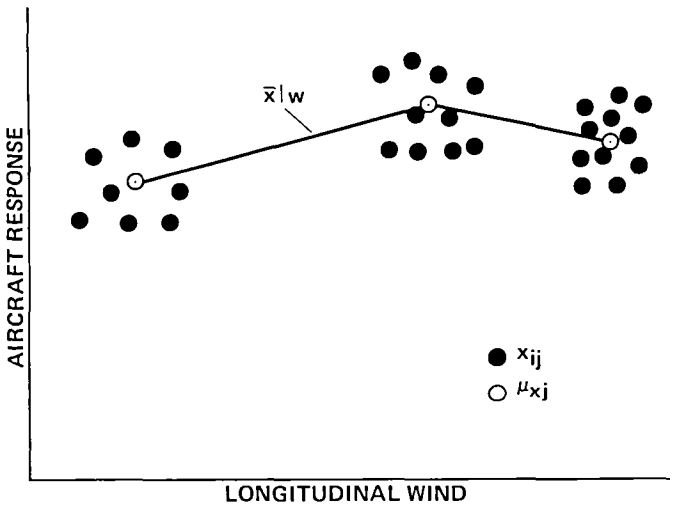

Sketch C1.– Determination of wind variation of statistical averages for "grouped" wind data.

To obtain the averaged values, for wind distributed more uniformly, a least squares curve fit of the quantities x and $(x-\mu_x)^2$ may be more appropriate as shown in sketch (C2) for $\bar{x}|w$. The former procedure was used for the reported results since, as described in the body of the report, the winds were grouped in this form.

As a first step in evaluating equations (C3) and (C4), the means and standard deviations for each wind group were obtained.

$$\bar{x}|w_j = \mu_{xj} = \frac{1}{N_j}\sum_{i=1}^{N_j} x_{ij} \qquad \text{(C5)}$$

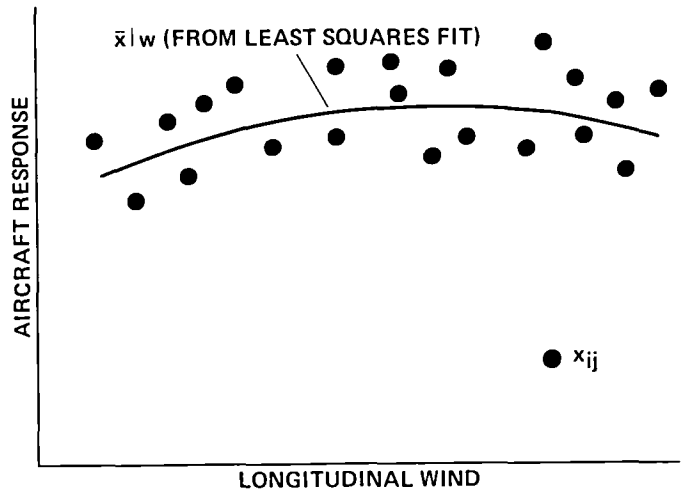

Sketch C2.– Determination of wind variation of statistical averages for "distributed" wind data.

$$\overline{(x-\mu_x)^2}|w_j = \sigma_{xj}^2 = \frac{1}{N_j}\sum_{i=1}^{N_j}(x_{ij}-\mu_{xj})^2 \qquad \text{(C6)}$$

where x_{ij} is the value of the aircraft response, x, for the ith approach occurring with the jth wind group, and N_j is the number of approaches for the jth wind group. These equations were used to compute means and standard deviations for aircraft responses at a particular altitude on the approach or at touchdown.

Statistical averages for aircraft response along the final approach were also obtained. First, means and standard deviations along each approach path in a group were calculated. Then the means and standard deviations of the path averages for the wind group were obtained. For the mean, equation (C5) was employed with $x_{ij} = \mu_{x_{ij}}$. For the standard deviation, two definitions were used. In one definition, which is the customary one, the rms, σ_{xj}, relative to the mean, μ_{xj}, for the group of approaches, N_j, was preferred in order to show average deviation from the group mean value.

$$\sigma_{xj} = \left\{\frac{1}{N_j}\sum_{i=1}^{N_j}\left[\sigma_{x_{ij}}^2 + (\mu_{x_{ij}} - \mu_{xj})^2\right]\right\}^{1/2} \qquad \text{(C7)}$$

where $\mu_{x_{ij}}, \sigma_{x_{ij}}$ are the mean and standard deviations of the x variable for the ith approach in the jth wind group, and

$$\mu_{xj} = \frac{1}{N_j}\sum_{i=1}^{N_j}\mu_{x_{ij}}$$

For the other definition, the rms of deviations about the mean for each approach was preferred in order to represent the average activity level occurring for the group of approaches

$$\sigma_{a_{xj}} = \left(\frac{1}{N_j} \sum_{i=1}^{N_j} \sigma_{x_{ij}}^2 \right)^{1/2} \tag{C8}$$

The numerical integration of equations (C3) and (C4) was performed as follows. The integration was divided into basic intervals depending on the values of wind for each group and intermediate intervals depending on the probability density function variations. Linear interpolation of the statistical averages for each wind group (eqs. (C5) and (C6) or (C7)) was used to obtain values for intermediate intervals. After employing a trapezoidal integration procedure for equations (C3) and (C4), coefficients dependent on the integration intervals and the wind probability density function were calculated and collected to form weighting factors for each wind group. Note that these coefficients are independent of the aircraft response. The equations for the combined wind statistical averages could then be expressed in the following form using the precalculated weighting factors.

$$\mu_x = \sum_{j=1}^{N_w} W_j \mu_{xj} \tag{C9}$$

$$\sigma_x = \left(\sum_{j=1}^{N_w} \left\{ W_j [\sigma_{xj}^2 + (\mu_{xj} - \mu_x)^2 \right] \right)^{1/2} \tag{C10}$$

where j denotes the summation relating to the wind; W_j is the weighting factor for the jth wind group with

$$\sum_{j=1}^{N_w} W_j$$

normalized to unity; and N_w is the number of wind groups. Note that the identifying subscripts, x and j, in the equations in the appendix are not used in the figures and tables discussed in the body of the report.

Numerical values of the weighting factors, W_j, were obtained for the following conditions. As was shown in the body of the report, the winds encountered in flight were clustered in three groups (head, low, and tail wind; $N_w = 3$). These winds, measured in the 152.4- to 30.5-m altitude range, were extrapolated to the 7.6-m reference altitude assuming the log-linear wind shear variation. This extrapolation resulted in a range from 7 knots (tail wind) to 9 knots (head wind) to be used with the wind distribution model. The model, together with the numerical integration steps, was then employed to determine the normalized weighting factors shown in the following table:

Wind, knots (h = 152.4 to 30.5 m)	-13 (head)	-1 (low)	10 (tail)
Weighting factor, W_j	0.303	0.564	0.133

In addition to determining means and standard deviations, these factors were also used to calculate the combined wind histograms presented in the body of the report with histogram frequency parameters in place of means in equation (C9).

APPENDIX D

EVALUATION OF MLS ERRORS

Radar tracking measurements of aircraft position were used to evaluate MLS accuracies. A description of the radar tracking capabilities is given in reference 20. Generally, the radar measurements provided a suitable reference for the final-approach region of interest except for the vertical position below altitudes of about 30 m. The determination and data processing of the MLS errors into a form for comparison with specifications, and the determination of the MLS noise error model for the simulation are provided in this section.

MLS Specification Data Processing

In this section, the determination of the MLS errors is outlined. Then, the processing of the MLS error data with specified filters, and the procedures for averaging the outputs for the comparisons with specifications shown in table 3 are described. The averaging procedures are intended to determine 4.5% P_e boundaries of the errors which are representative of the period in which flight testing was performed.

The MLS errors were calculated by the following sequence. The radar measurements of aircraft position were first transformed to rectangular position coordinates oriented with respect to the runway heading. This initial step was digitally processed in real time during the flight while all subsequent data analysis was performed postflight. The first postflight step consisted of smoothing the rectangular radar coordinates in the manner described in appendix C. The smoothed radar was then transformed to the MLS coordinates with the azimuth and elevation angles in planar and conical form, respectively. The MLS coordinate errors were defined as follows:

$$\text{MLS error, } \Delta x_i = x_{i\text{MLS}} - x_{i\text{radar}} \tag{D1}$$

The MLS errors were processed through use of the MLS specification filters shown in figure D1. Use of these filters allowed consideration of dynamic content in the accuracy specifications. The specifications were given as 4.5% P_e values of the filter outputs. The smoothing filter (fig. D1) represents the minimum cut-off frequency that is allowed by the airborne receiver filtering and hence was not included in the postflight data processing. Note that the output of the path-following filter includes the very low frequency or bias component. Although the specifications for the MLS installation at the flight-test site (ref. 19) included a value for the bias in addition to the PFE, the bias has been omitted in subsequent MLS specifications. Maintaining the distinction of the bias portion of the PFE for the results in this report was desirable since the bias portion of the errors was obtained from the limited flight-test evaluation period and may not have been typical for the installation, distorting the path-following results.

The MLS errors were evaluated on the 6° final approach over the altitude range between 152.4 and 30.5 m. Because time did not permit the determination of the filtered outputs for all approaches made, the following approximate procedure was used. The MLS (unfiltered) errors for every approach were processed to obtain the bias and standard deviation (noise). For selected approaches (about 10%), the errors were further processed with the PF and CM filters. An examination of the bias and noise levels for the unfiltered errors indicated that the bias had a day-to-day variation whereas the noise magnitude did not show any trend during the test period. In order to best relate the available bias and noise results to operational usage, the following procedure was employed. Bias results were weighted so that each day's results would have the same contribution to the overall bias regardless of the number of approaches made. The unfiltered noise average, σ_t, was based directly on the unweighted rms of all of the approaches. These relations are represented by the following equations:

Bias:

$$\mu_{\text{bias}} = \frac{1}{N_d} \sum_{j=1}^{N_d} \frac{1}{N_j} \sum_{i=1}^{N_j} \mu_{ij} \tag{D2}$$

$$\sigma^2_{\text{bias}} = \frac{1}{N_d} \sum_{j=1}^{N_d} \frac{1}{N_j} \sum_{i=1}^{N_j} (\mu_{ij} - \mu_{\text{bias}})^2 \tag{D3}$$

where μ_{ij} is the bias for the ith approach on the jth day, N_j is the number of approaches on the jth day, and N_d is the number of days.

Unfiltered Noise:

$$\sigma_t^2 = \frac{1}{\sum_{j=1}^{N_d} N_j} \left(\sum_{j=1}^{N_d} \sum_{i=1}^{N_j} \sigma_{ij}^2 \right) \tag{D4}$$

where σ_{ij} is the unfiltered noise (MLS error with the bias removed) for the ith approach on the jth day.

The standard deviation of the resultant short- and long-term (assumed independent) random components of the unfiltered MLS error, σ_{total}, is given by the following equation:

$$\sigma_{total} = (\sigma_{bias}^2 + \sigma_t^2)^{1/2} \quad \text{(D5)}$$

The standard deviation of the resultant short- and long-term path-following error, σ_{PF}, is given by the following equation:

$$\sigma_{PF} = (\sigma_{bias}^2 + K_{PF}^2 \sigma_t^2)^{1/2} \quad \text{(D6)}$$

where K_{PF} is the average ratio of PFN to unfiltered noise obtained from the *PF*-filter-processed approaches. The standard deviation of the control motion noise, σ_{CMN}, is dependent only on a short-term random component.

$$\sigma_{CMN} = K_{CM} \sigma_t \quad \text{(D7)}$$

where K_{CM} is the average ratio of CMN to unfiltered noise obtained from the *CM*-filter-processed approaches.

The previously described quantities were used to obtain the average bias, μ_{bias}, and as a basis for calculating the 4.5% P_e ($2\sigma_p$) values shown in table 3. The $2\sigma_p$ values for bias, path following, and total errors were calculated, assuming gaussian distributions, from the mean, μ_{bias}, and the respective standard deviations, σ_{bias}, σ_{PF}, and σ_{total}. The $2\sigma_p$ value for CMN was obtained directly from $2\sigma_{CMN}$ (eq. (D7)) since no bias was involved for this higher frequency error component. Note that the number of flight days (13) limited the accuracy of the statistical calculations for bias. However, the results are considered representative of the period encountered and are in a form comparable with the specifications.

MLS Error Model for Simulation

The error model used was as simple a form as feasible, since time did not permit an extensive dynamic analysis of the MLS error data. The form selected was of white noise passed through a first-order filter. For this model, only two parameters were required, the noise magnitude and the first-order time constant. Values for these parameters were obtained as follows. As previously mentioned, the error data for all approaches were analyzed to obtain the bias plus the standard deviation of the error (noise). The average standard deviation, σ_t (eq. (D4)), provided the magnitude of the noise filter output. For selected approaches (about 15%), the autocorrelation function of the noise was obtained. A least squares fit of a first-order exponential function was made to the autocorrelation function for each approach. The average value of the constants from the exponential function fits provided the time constant for the noise filter. The separation of the error into noise and bias allowed use of the simulation to generate effects of noise only or, when desired, to add a bias value to match conditions on a particular flight. The MLS results from the simulation given in this report show only the effects of noise on the aircraft response. Note that the total noise spectrum contains frequency components in both the path-following and control motion ranges and that the exponential fit should reflect this distribution. The further separation of the MLS noise model into path-following and control motion components is discussed in the body of the report.

REFERENCES

1. Neuman, Frank; Watson, Delamar M.; and Bradbury, Peter: Operational Description of an Experimental Digital Avionics System for STOL Airplanes. NASA TM X-62448, 1975.
2. Feinreich, B.; Degani, O.; and Gevaert, G.: Development and Evaluation of Automatic Landing Control Laws for Light Wing Loading STOL Aircraft. NASA CR-166160, 1981.
3. Morrison, John A.: Operational Requirements for Flight Control and Navigation Systems for Short Haul Transport Aircraft. NASA CR-137975, 1976.
4. Spangler, Roman M.: Simulated Ground-Level STOL Runway/Aircraft Evaluation. FAA-RD-73-110, 1973.
5. Rosewarne, H. P.; and Spruston, D. D.: The Canadian STOL Demonstration – The Data Collection, The Findings and Their Applications. The 10th ICAS Conference, Paper 76-53, October 1976.
6. Bentham, Richard P.: Some DHC-6 Twin Otter Approach and Landing Experience in a STOL System. AGARD-CP-160, 1974.
7. Anon.: Ransome Begins Dash 7 Service Today. Business Aviation, October 16, 1979, p. 123.
8. Anon.: Special Conditions for de Havilland Aircraft of Canada Model DHC-7 Airplane. FAA Special Conditions, No. 25-53-EA-10, 1973.
9. Scott, B. C.; Hynes, C. S.; Martin, P. W.; and Bryder, R. B.: Progress Toward Development of Civil Airworthiness Criteria for Powered-Lift Aircraft. NASA TM X-73,124, 1976.
10. Watson, D. M.; Hardy, G. H.; Moran, J. F.; and Warner, D. N., Jr.: A Method for Determining Landing Runway Length for a STOL Aircraft. 1980 Aircraft Safety and Operating Problems. NASA Conference Publication CP-2170, Part 1, Nov. 5-7, 1980, pp. 127-144.
11. 1975 Ride Quality Symposium, Williamsberg, Va., August 11-12, 1975, DOT-TSC-OST-74-40, NASA TM X-3295.
12. Jacobson, I. D.: Construction and Verification of a Model Passenger Response to STOL Aircraft Characteristics. SAE Preprint 760525, 1976.
13. Jacobson, Ira D.; Kuhlthau, A. Robert; and Richards, Larry G.: Passenger Ride Quality in Transport Aircraft. AIAA Journal of Aircraft, vol. 15, no. 11, November 1978.
14. Gordon, C. K.; and Dodson, R. O.: STOL Ride Control Feasibility Study. NASA CR-2276, 1973.
15. Wehrend, W. R., Jr.; and Meyer, George: Flight Tests of the Total Automatic Flight Control System (TAFCOS) Concept on a DHC-6 Twin Otter Aircraft. NASA TP-1513, 1980.
16. Anon.: Criteria for Approval of Category IIIa Landing Weather Minima. FAA Advisory Circular 120-28B, 1977.
17. Anon.: Automatic Landing Systems. FAA Advisory Circular 20-57A, 1971.
18. Anon.: Planning and Design Criteria for Metropolitan STOL Ports. FAA Advisory Circular 150/5300-8, 1965.
19. Burrous, C. N.; and Narimatsu, R.: Site Preparation and Installation of the Prototype Texas Instruments Basic Narrow Configuration Microwave Landing System. NASA TM-78588, 1979.
20. Warner, David N., Jr.; and Moran, Francis J.: Flight-Test Evaluation Errors in the MODILS and TACAN Navigation Aids at NALF Crows Landing. NASA TM-78584, 1979.
21. Anon.: International Standards and Recommended Practices, Aeronautical Telecommunications, Annex 10, ICAO, Chapter 3, 1974.
22. Anon.: British Air Registration Requirements, Paper no. 367, Issue 3, June 1970.
23. Chalk, C. R.; Neal, T. P.; Harris, T. M.; Prichard, F. E.; and Woodcock, R. J.: Background Information and User Guide for MIL-F-8785B(ASG), Military Specifications – Flying Qualities of Piloted Airplanes. AFFDL TR-69-72, 1969.
24. Kelley, R. J.: Guidance Accuracy Considerations for the Microwave Landing System. Navigation, vol. 24, no. 3, Fall 1977.
25. Kelley, R. J.; and LaBerge, E. F. C.: Guidance Accuracy Considerations for the Microwave Landing System Precision DME. Navigation, vol. 27, no. 1, Spring 1980.
26. Hansen, Q. M.; Young, L. S.; Rouse, W. E.; and Osder, S. S.: Development of STOLAND, a Versatile Navigation, Guidance and Control System. AIAA Paper 72-789, 1972.
27. Blakelock, John H.: Automatic Control of Aircraft and Missiles. John Wiley, New York, 1965.

TABLE 1.– ONBOARD MEASURED WINDS FOR THE 152.4- TO 30.5-m ALTITUDE RANGE

Wind group	Number of approaches	Wind component, knots					
		Longitudinal			Lateral		
		Wind		Turbulence	Wind		Turbulence
		μ	σ	σ_a	μ	σ	σ_a
Head	14	-13	1.2	1.5	14	1.8	1.5
Low	39	-1	3.5	.8	2	2.2	.9
Tail	29	10	1.7	1.1	-4	3.8	1.3
Combined	---	-2.7	7.9	1.1	---	---	---

TABLE 2.– GROUND-MEASURED WINDS AT 4.7-m ALTITUDE

Wind group	Number of approaches	Wind component, knots			
		Longitudinal		Lateral	
		μ	σ	μ	σ
Head	14	-9	1.6	7	1.8
Low	39	-3	2.1	0	1.4
Tail	29	6	2.9	-4	2.8

TABLE 3.– COMPARISON OF FLIGHT-MEASURED MLS ERRORS IN THE 152.4- TO 30.5-m ALTITUDE RANGE WITH SPECIFICATIONS

Error source	Elevation, deg		Range, m	
	Measured	Specification	Measured	Specification
Bias μ	0.04	---	-9.2	---
Bias $2\sigma_p$	.09	0.09	19.4	---
PFE, $2\sigma_p$	.11	.14	19.7	---
CMN, $2\sigma_p$	.04	.05	3.4	---
Total error, $2\sigma_p$	0.12	---	20.1	30.5

TABLE 4.– CHARACTERISTICS OF MLS NOISE MODEL

MLS error	Matched results from flight		Ratio of specification filter to total noise	
	σ_t	Time constant, sec	σ_{PF}/σ_t	σ_{cm}/σ_t
Elevation error	0.03	3.0	0.86	0.61
DME error	2.1	.4	.57	.80

TABLE 5.– GLIDEPATH TRACK ERRORS FROM FLIGHT RESULTS

Wind	Glidepath track error, m					
	152.4-m altitude		30.5-m altitude		Flare initiation	
	μ	2σ	μ	2σ	μ	2σ
Head	0.2	1.6	0.1	1.8	-0.5	1.8
Low	-.1	1.7	-.1	1.3	.2	1.3
Tail	-.7	1.2	.1	1.5	-.2	1.6
Combined	-0.1	1.6	0	1.6	-0.1	1.7

TABLE 6.– COMPARISON OF FLIGHT RESULTS, SIMULATION RESULTS, AND PERFORMANCE CRITERION FOR GLIDEPATH TRACK ERRORS FOR THE ALTITUDE RANGE, 152.4 TO 30.5 m

Data source	Glidepath track error, m, $2\sigma_p$
Flight:	
Combined wind	1.6
Simulation:	
Turbulence model	1.6
MLS noise	.8
Turbulence + MLS noise	1.8
CTOL performance criterion (ref. 16)	3.7

TABLE 7.– VERTICAL DEVIATION OF AIRCRAFT FROM FINAL-APPROACH PATH, 4.5% P_e VALUES

Distance from GPIP, m	290	1450
Description	Vertical deviation, m	
MLS elevation bias error (flight), $2\sigma_p$	0.5	2.3
Turbulence + MLS noise (simulation)	1.7	1.7
Total deviation	1.8	2.9

TABLE 8.– COMPARISON OF PITCH ATTITUDE FROM FLIGHT AND FROM SIMULATED MLS NOISE WITH THE ICAO ILS NAVIGATION ERROR CRITERION (REF. 21)

Data source	Pitch attitude $2\sigma_p$, deg
Flight (at flare initiation):	
Head wind	1.6
Low wind	1.2
Tail wind	1.7
Simulation:	
MLS noise	0.4
Navigation error criterion	2.0

TABLE 9.– COMPARISON OF VERTICAL ACCELERATION OBTAINED FROM FLIGHT AND SIMULATION RESULTS WITH RIDE COMFORT LIMIT; 152.4- TO 30.5-m ALTITUDE RANGE

Data source	Vertical acceleration σ_a, g
Flight:	
Combined wind	0.038
Simulation:	
MLS noise	.019
Turbulence model	.029
Turbulence + MLS	.035
Vertical portion of acceptable ride comfort limit (ref. 13)	.06

TABLE 10.– CALIBRATED AIRSPEED ERRORS FROM FLIGHT RESULTS

Wind	Calibrated airspeed error, knots					
	152.4-m altitude		30.5-m altitude		Flare initiation	
	μ	2σ	μ	2σ	μ	2σ
Head	0.2	1.9	-0.1	2.2	0.8	3.0
Low	.7	2.0	-.3	1.6	-.1	1.6
Tail	.8	2.2	-.4	1.5	-.4	2.2
Combined	0.6	2.1	-0.3	1.8	0.1	2.2

TABLE 11.– COMPARISON OF AIRSPEED ERRORS FROM FLIGHT AND SIMULATION WITH PERFORMANCE CRITERION, 152.4- TO 30.5-m ALTITUDE RANGE

Data source	Airspeed error, knots $2\sigma_p$
Flight:	
Combined wind	1.9
Simulation:	
Turbulence model	2.1
MLS noise	.2
Turbulence + MLS	2.2
CTOL performance criterion (ref. 16)	5.0

TABLE 12.– STATISTICAL AVERAGES OF FLIGHT RESULTS AT TOUCHDOWN

Measurements	Wind	μ	σ
Radar-measured longitudinal position, m	Head	13	18
	Low	66	16
	Tail	87	23
	Combined	53	33
Sink rate, mps	Head	-1.4	.3
	Low	-1.0	.2
	Tail	-.9	.2
	Combined	-1.1	.3
Pitch attitude, deg	Head	3.1	1.0
	Low	.5	.7
	Tail	.6	.8
	Combined	1.3	1.4
Calibrated airspeed, knots	Head	62.1	1.3
	Low	61.9	1.3
	Tail	62.8	1.6
	Combined	62.1	1.4

TABLE 13.– COMPARISON OF FLIGHT RESULTS AT TOUCHDOWN WITH DESIGN GOALS

Design goals (2σ)	Flight (combined wind histogram)
$(x_{td_{long}} - x_{td_{short}}) \leqslant 152$ m	131
$\dot{h} \geqslant -1.8$ mps	-1.8
$\theta > -0.5$ deg	-.7

TABLE 14.– COMPARISON OF LONGITUDINAL RANGE DISPERSIONS WITH OTHER TWIN OTTER FLIGHT-TEST RESULTS

Data source	Standard deviation, m	Number of approaches
NASA Ames, automatic	33	82
NAFEC (ref. 4), manual	28	267
CATA (ref. 5), manual	41	852

TABLE A1.– CONSTANTS FOR CONTROL LAWS AND FILTERS FOR FINAL-APPROACH TRACKING

(a) Control law parameters

Path error pitch command:

$F_g(s) = [(K_{ih}/s) + K_h]\,\Delta\hat{h} + K_{dh}\Delta\dot{\hat{h}}$

where

K_{ih} = -0.0912 deg/m-sec, -0.0278 deg/ft-sec

K_h = -1.093 deg/m, -0.333 deg/ft

K_{dh} = -3.645 deg/mps, -1.111 deg/fps

Pitch stability augmentation:

K_θ = 1.2 deg/deg

K_q = 0.9 deg/deg/sec

q_{ref} = 1532 N/m^2, 32.0 psf

Airspeed control:

$F_v(s) = K_{vt}\hat{V}_e - K_{a_x}a_x + K_{it}(V_e/s)$

where

K_{vt} = 0.330 cm/knot, 0.13 in./knot

K_{a_x} = 1.583 cm/m/sec^2, 0.19 in./fps^2

K_{it} = 0.203 cm/knot-sec, 0.008 in./knot-sec

$K_{\dot{T}}$ = 1.0 sec^{-1}

(b) Complementary filter parameters

Position filters:

All vertical and horizontal position filters are third order. The feedback gains form a triple pole, $(s + \omega)^3$, by means of the following relations:

$K_{position} = 3\omega$

$K_{rate} = 3\omega^2$

$K_{accel} = \omega^3$

Δh filter frequency, ω, rad/sec:

$\omega = 0.1$ for $\hat{x} \leqslant -3048$

$\omega = 0.1 + \dfrac{0.2(\hat{x} + 3048)}{1524}$ for $-3048 \geqslant \hat{x} \leqslant -1524$

$\omega = 0.3$ for $\hat{x} \geqslant -1524$

where

$\hat{x}$ is the complementary filtered longitudinal distance from the elevation phase center, m.

Radio altimeter filter for flare:

ω = 0.6 rad/sec

Airspeed filter:

The feedback gains for the second-order filter form a double pole, $(s + \omega)^2$, with ω = 0.5 rad/sec.

$K_{v1} = 1/8$

$K_{v2} = 1/2$

TABLE A2.– CONSTANTS USED AND EVALUATED AT FLARE INITIATION

Flare initiation constants (eq. (A1)):

h_{fo} = 5.27 m, 17.3 ft
K_{fdh} = 2.5 sec
K_{fv} = 8.26 m, 27.1 ft

Flare guidance constants calculated at flare initiation:

Velocity ratio limits:

$(\hat{V}_{co}/V_{Go})_{ul} = (\hat{V}_{co}/V_{Go})$ with upper limit of 1 (<1 for tail wind)

$(\hat{V}_{co}/V_{Go})_{ll} = (\hat{V}_{co}/V_{Go})$ with lower limit of 1 (>1 for head wind)

Velocity error equation:

ΔV_o(knots) = $V_b - \hat{V}_{col}$

where

V_b = 66 + 0.0066(W_{ac} - 4990)

W_{ac} = aircraft weight in kg

$\hat{V}_{col} = \hat{V}_{co}$ with lower limit of 68 knots

TABLE A3.– FLARE GUIDANCE GAINS AND CONSTANTS

Closed-loop path guidance:

$\dot{h}_{td}$ = 0.686 mps, -2.25 fps
K_{hf} = 3.28 deg/m, 1.0 deg/ft
K_{hdf} = 9.91 deg/mps, 3.02 deg/fps
T_c = 0.65 sec
K_4 = 0.44
K_{ih} = 0.721
h_i = 3.81 m, 12.5 ft
K_{a_z} = 0.623 deg/mps^2, 0.19 deg/fps^2
T_g = 1.0 sec

Altitude driving function:

θ'_{cb} = 3.25 deg
$K_{g\theta}$ = 0.05

Theta prediction:

θ^c_{TD} = 3.6 deg
T_{θ_p} = 2.0 sec

Elevator prediction:

K_{hep} = 0.732
K_{ep_1} = 0.236
K_{ep_2} = 0.0953
K_{ep_3} = 0.223
K_{evo} = 0.00727 deg/knot
K_{ev} = 0.0727 deg/knot
T_{ep} = 0.33 sec

Pitch stability augmentation:

K_{θ_f} = 2.4 deg/deg
K_{q_f} = 2.3 deg/deg/sec

Throttle control:

K_{dhT} = 0.104 cm/sec/mps, 0.0125 in./sec/fps
$\dot{h}_B$ = -3.81 mps, -12.5 fps
K_{vtf} = 0.127 cm/sec/knot, 0.05 in./sec/knot

Figure 1.– Twin Otter test aircraft.

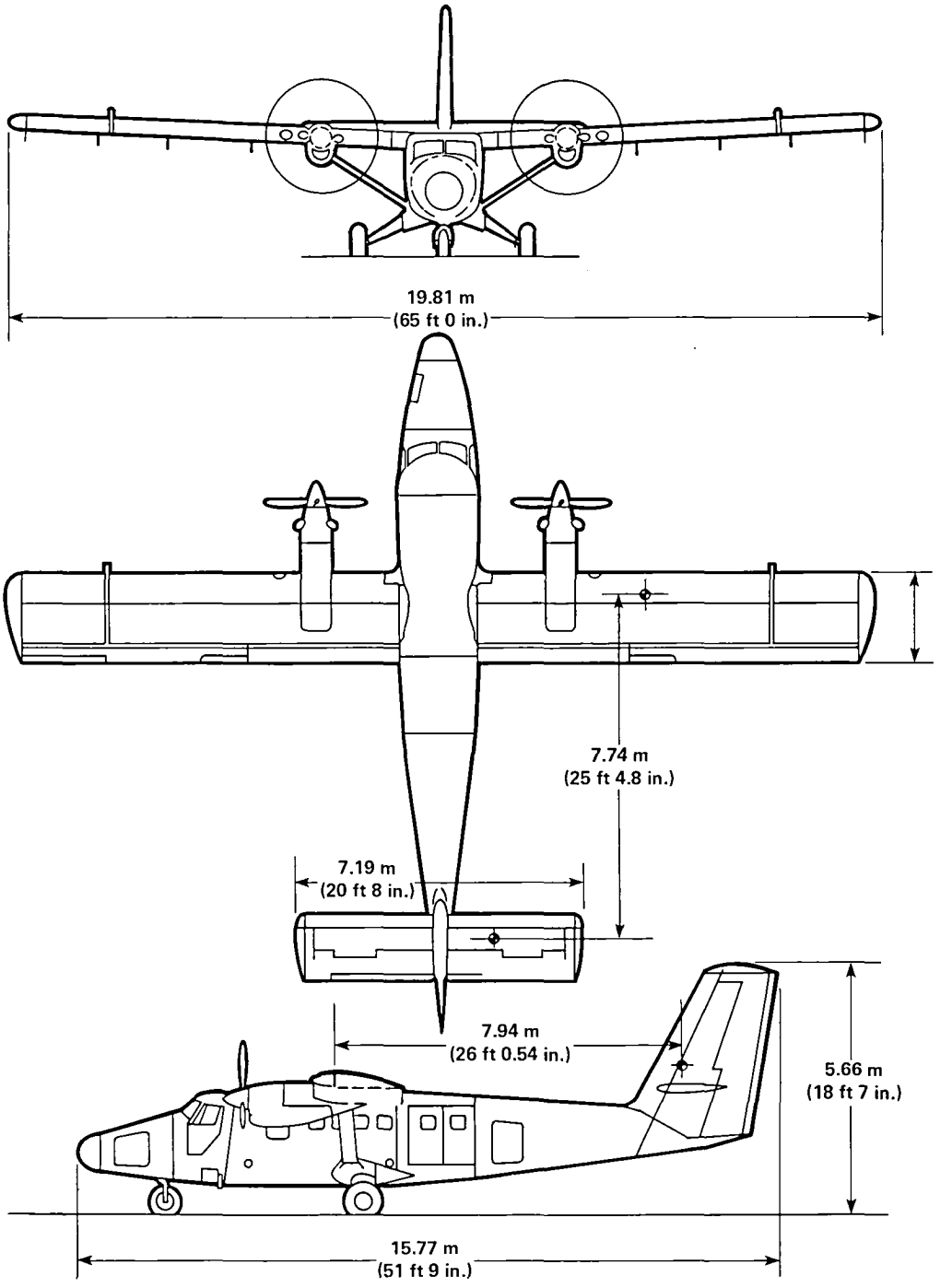

Figure 2.– Three-view drawing of test aircraft.

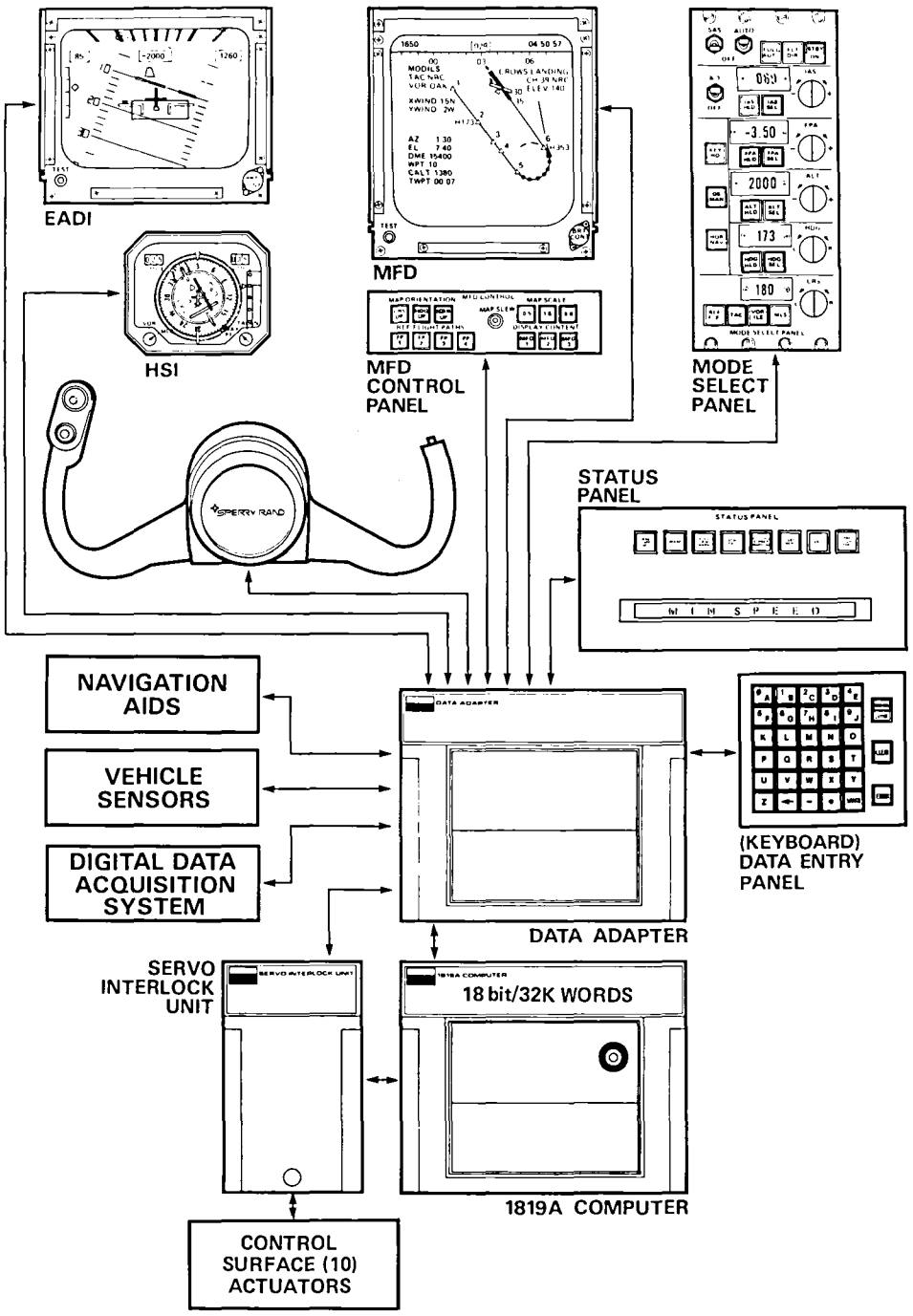

Figure 3.– STOLAND research avionics system.

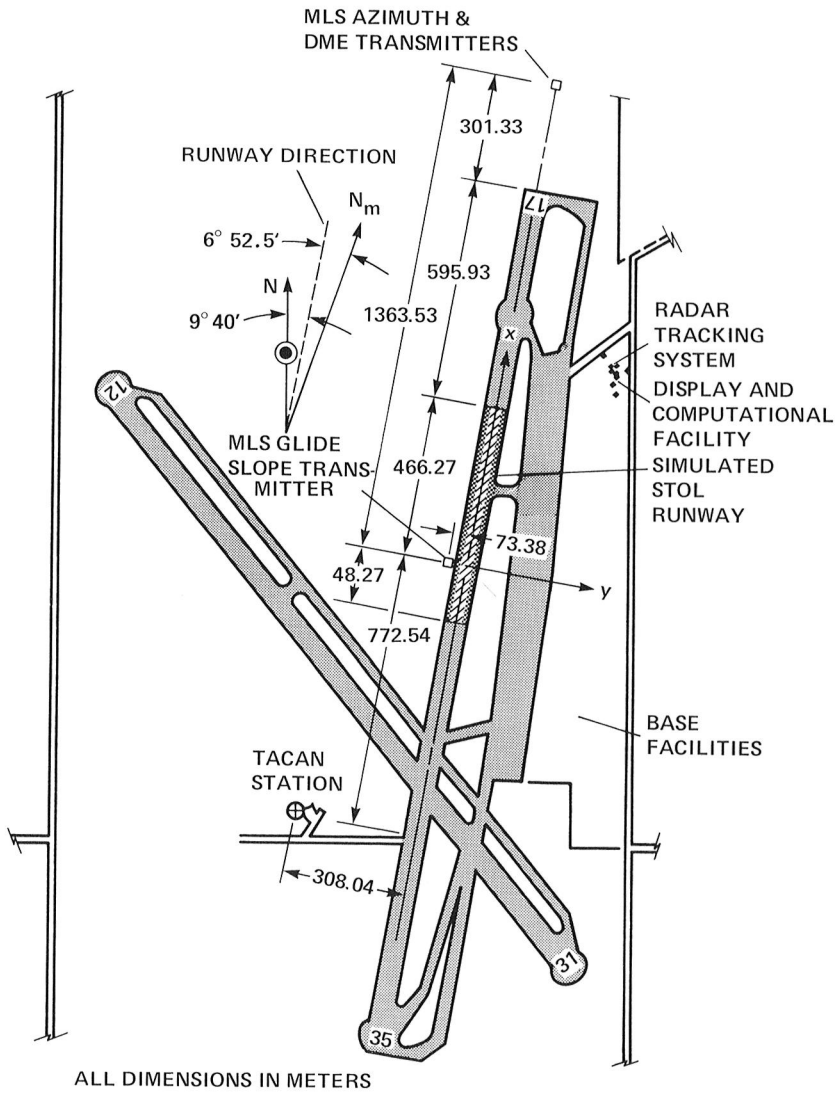

Figure 4.– Ground support equipment deployment at Crows Landing.

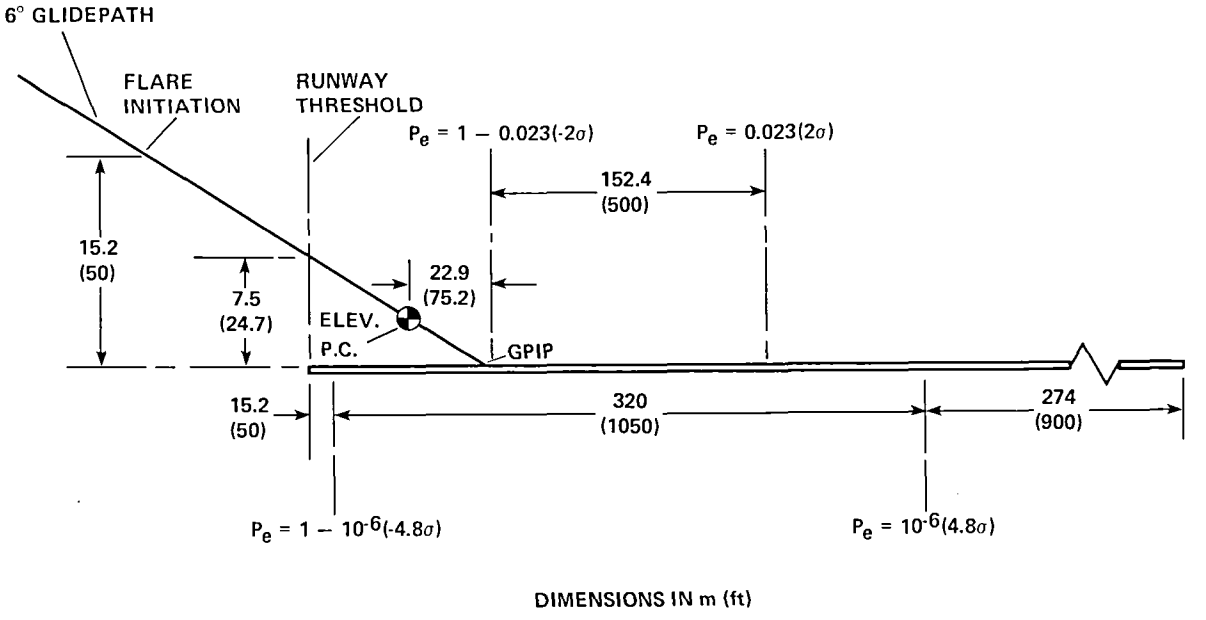

Figure 5.– Touchdown geometry and longitudinal dispersion criteria for STOLport.

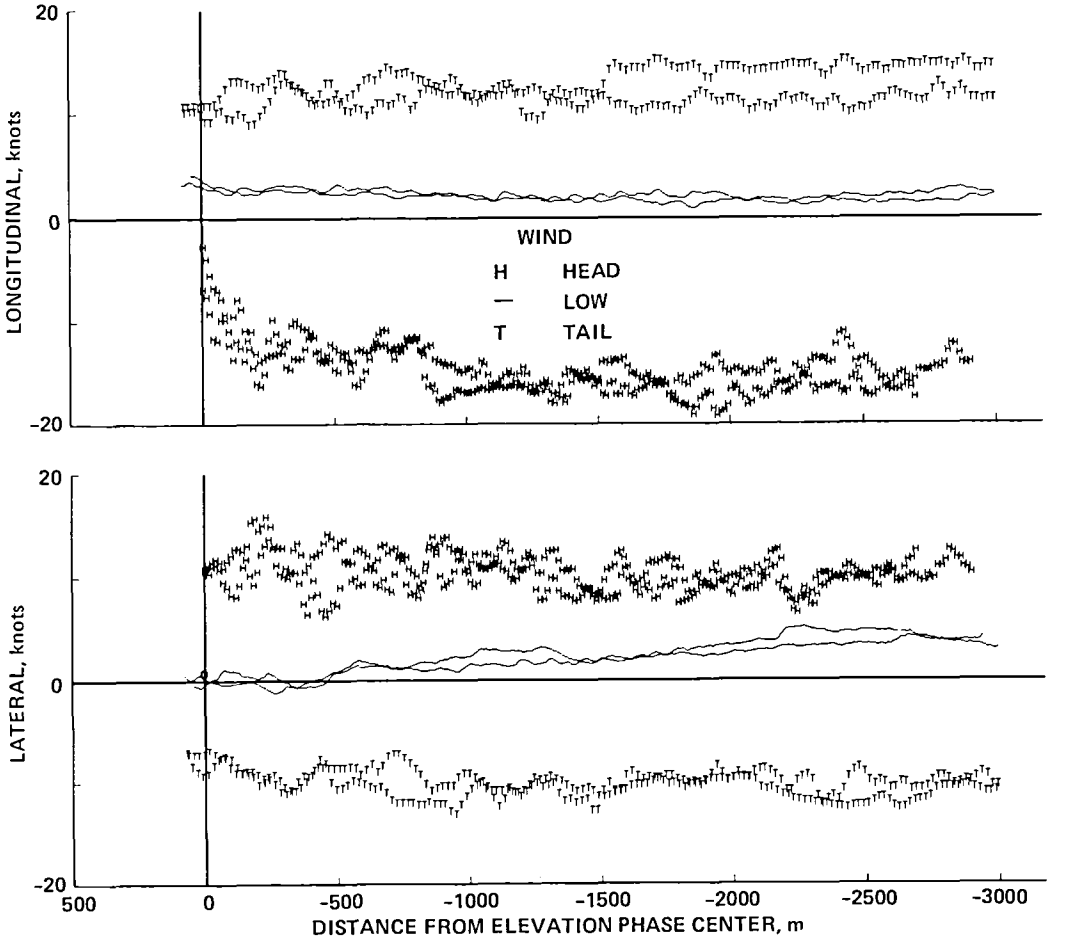

Figure 6.– Typical wind variations on the final approach.

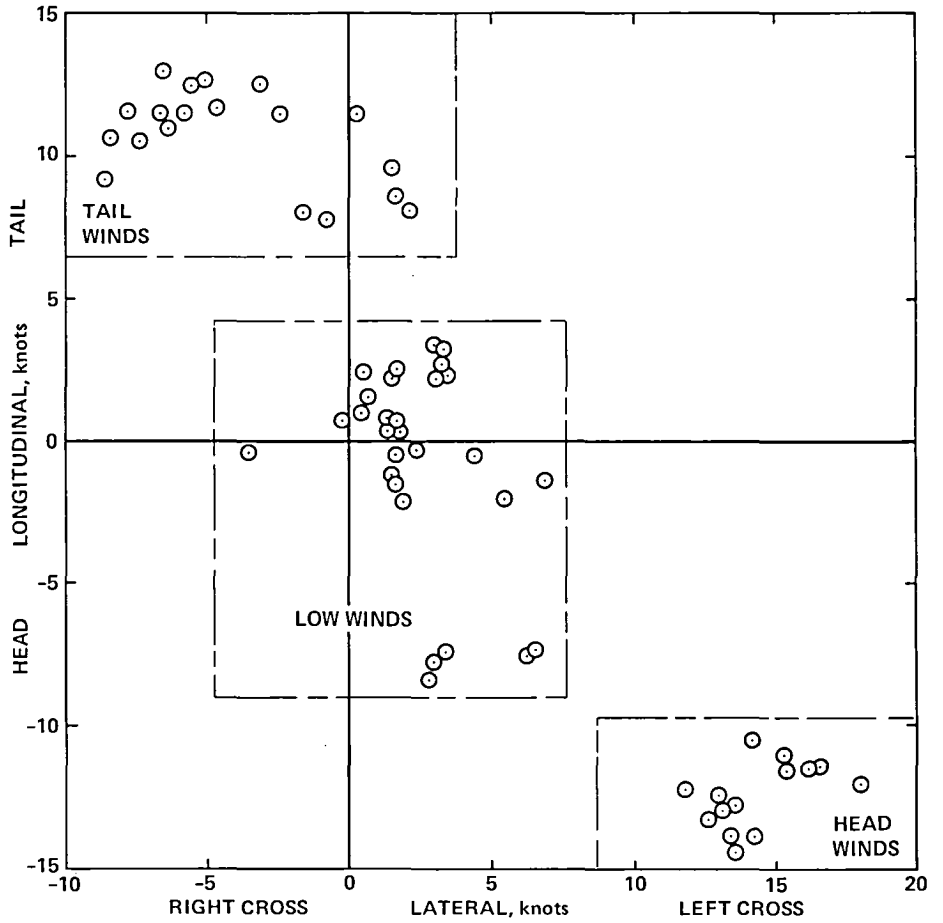

Figure 7.— Onboard-measured wind for the 152.4- to 30.5-m altitude range.

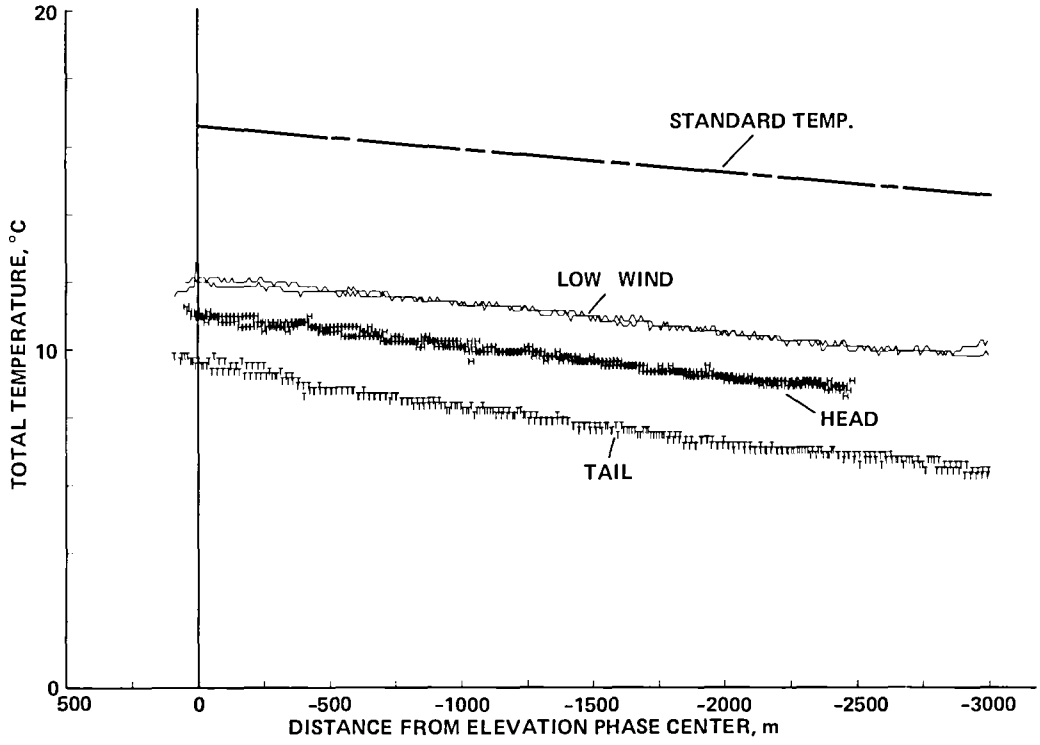

Figure 8.– Typical temperature variations on the final approach for the three wind conditions.

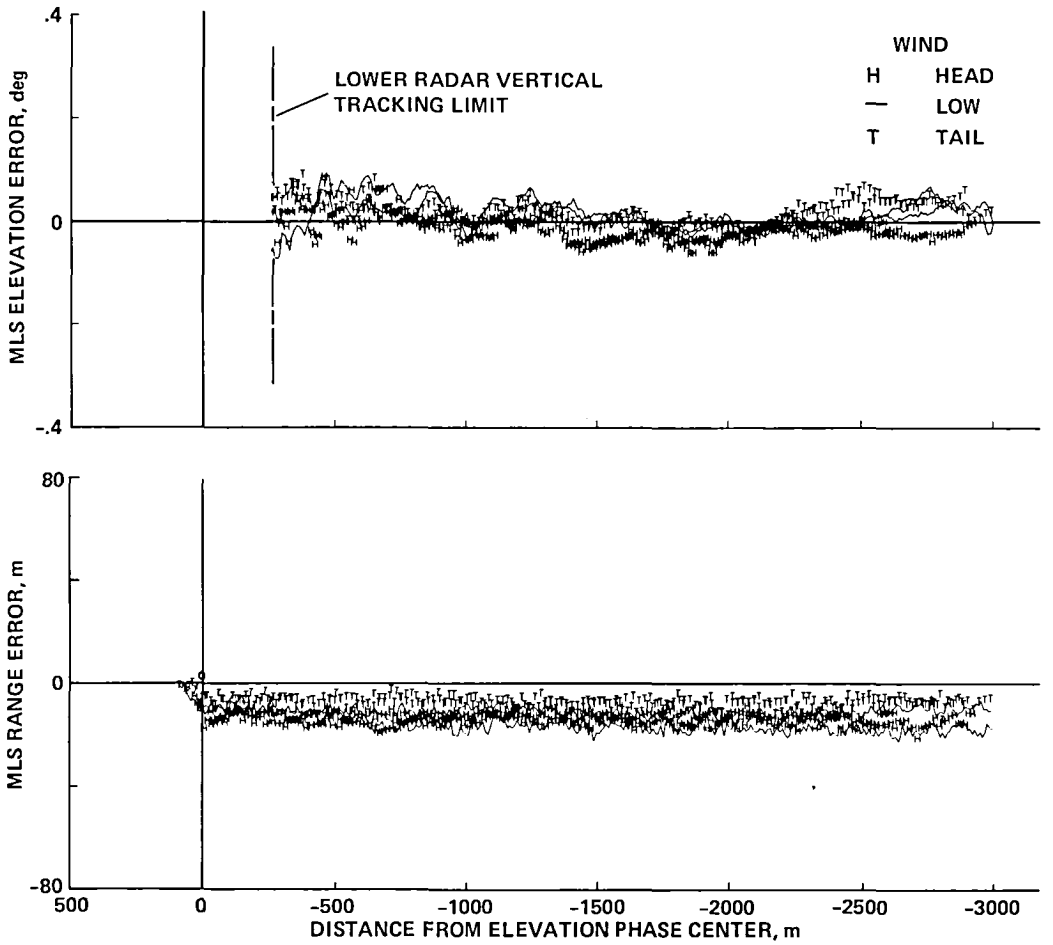

Figure 9.– Typical variations in MLS errors on the final approach.

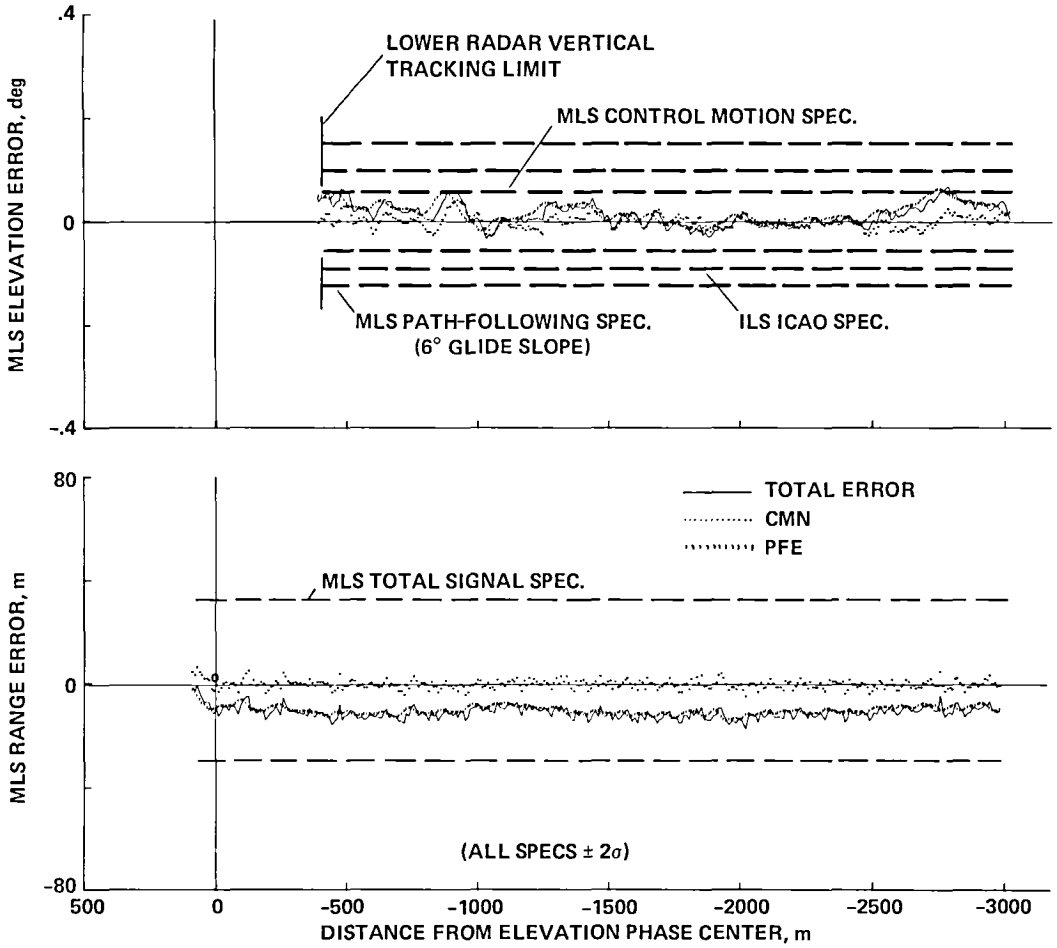

Figure 10.– Typical comparison of MLS errors on the final approach with specifications.

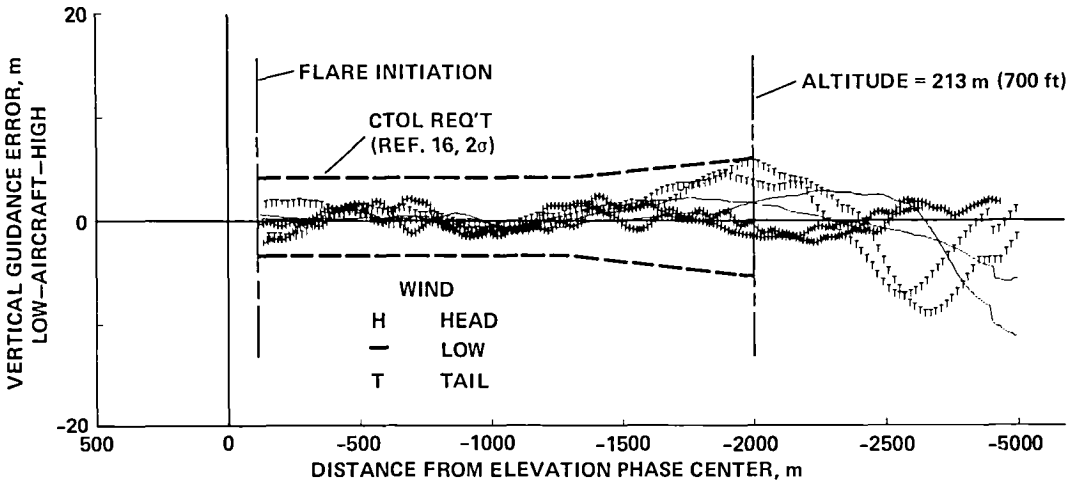

Figure 11.– Typical variations in glidepath track errors.

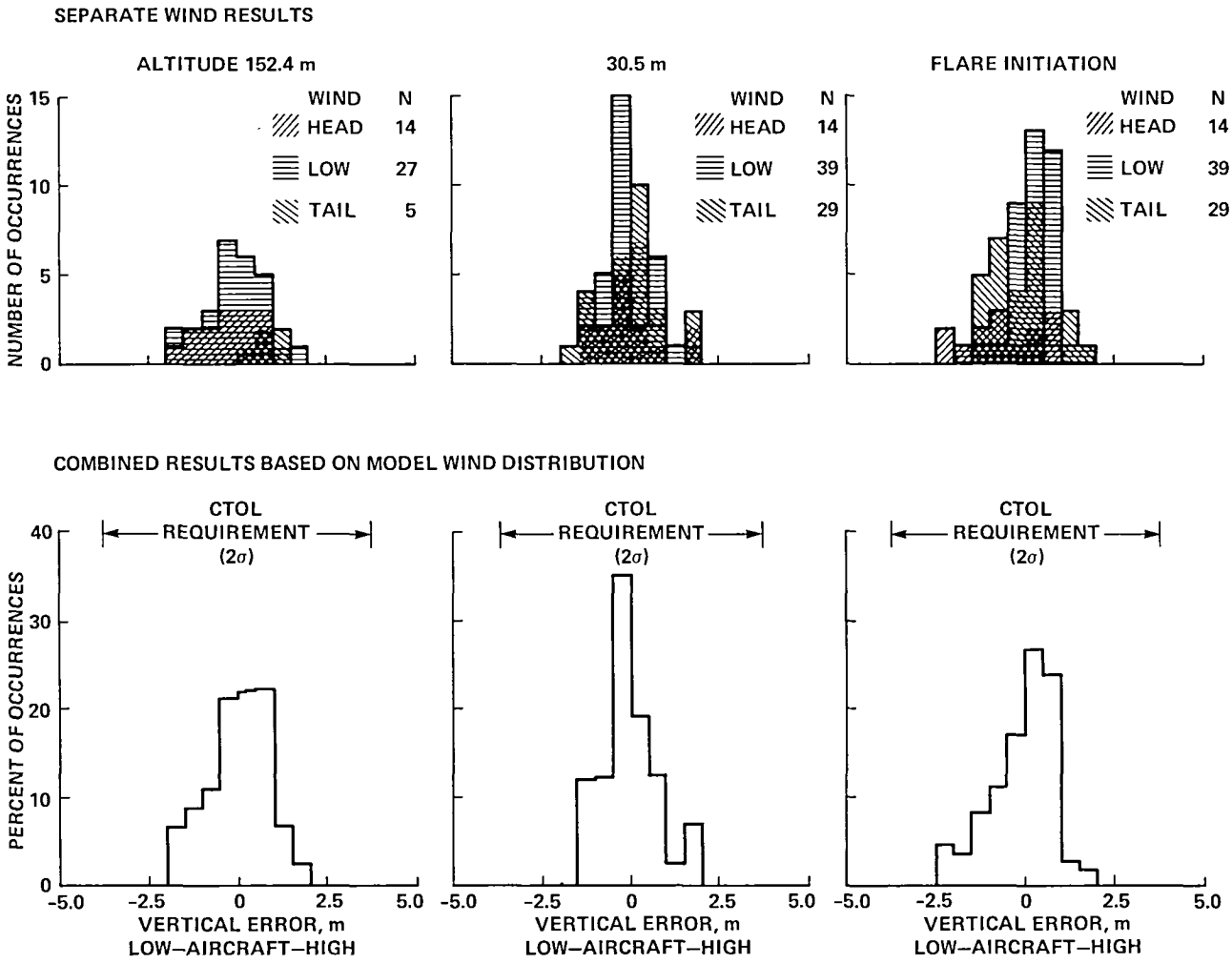

Figure 12.– Distributions of glidepath track errors at three altitudes.

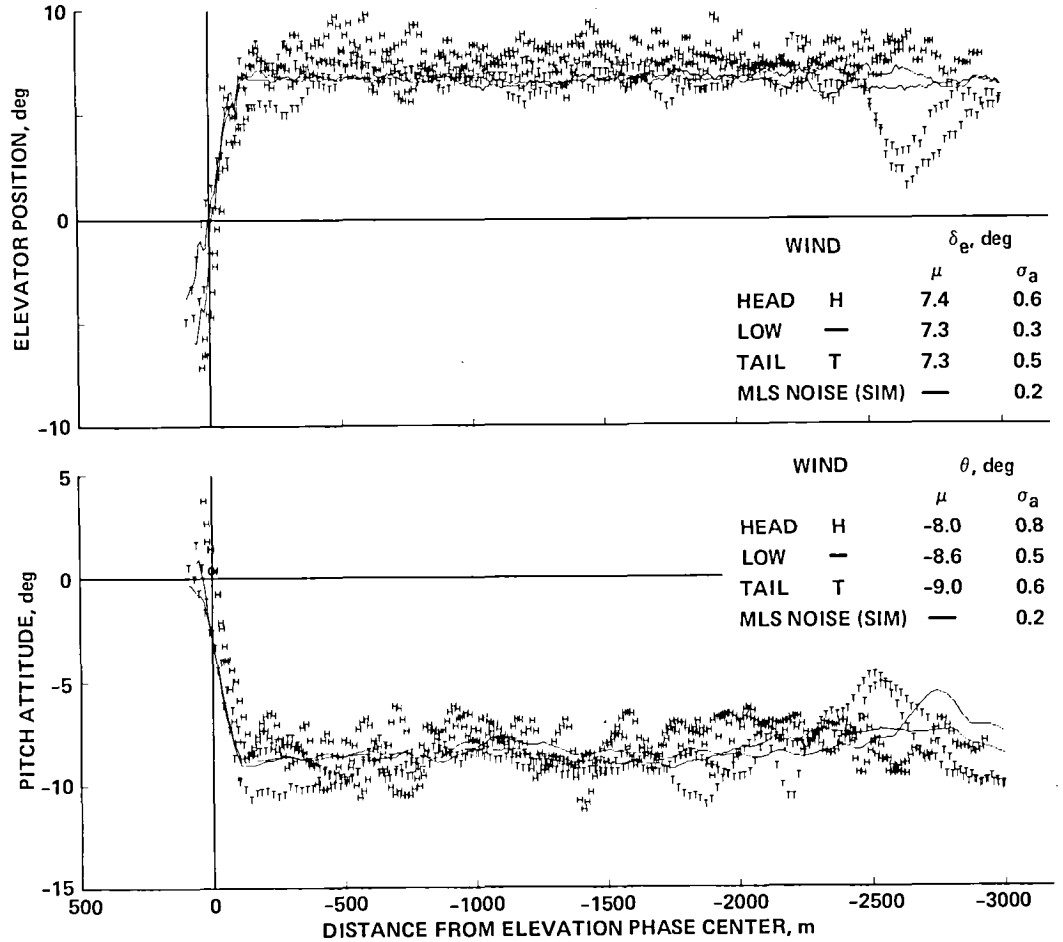

Figure 13.– Typical variations and statistical averages for glidepath track control variables.

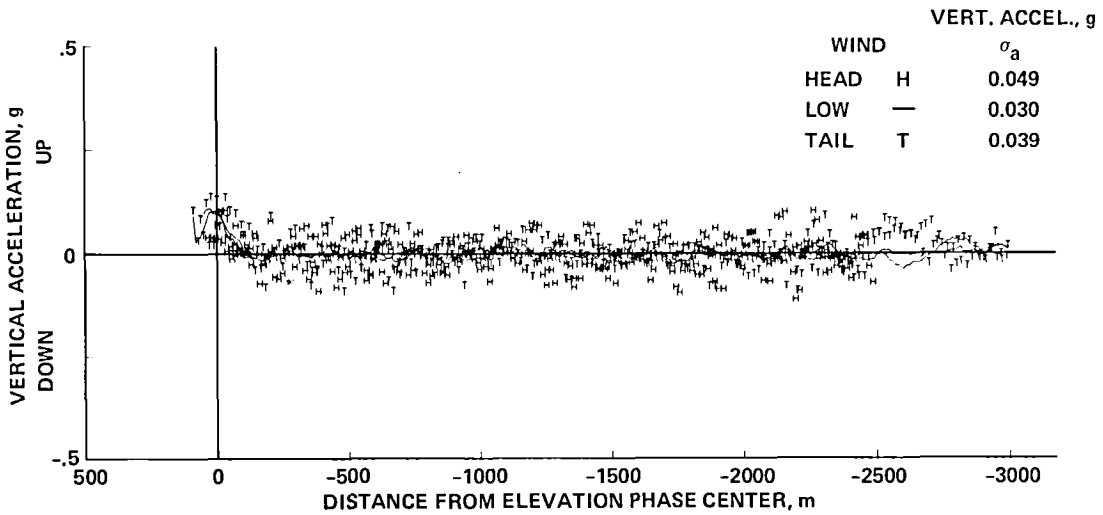

Figure 14.– Typical variations and statistical averages for vertical acceleration.

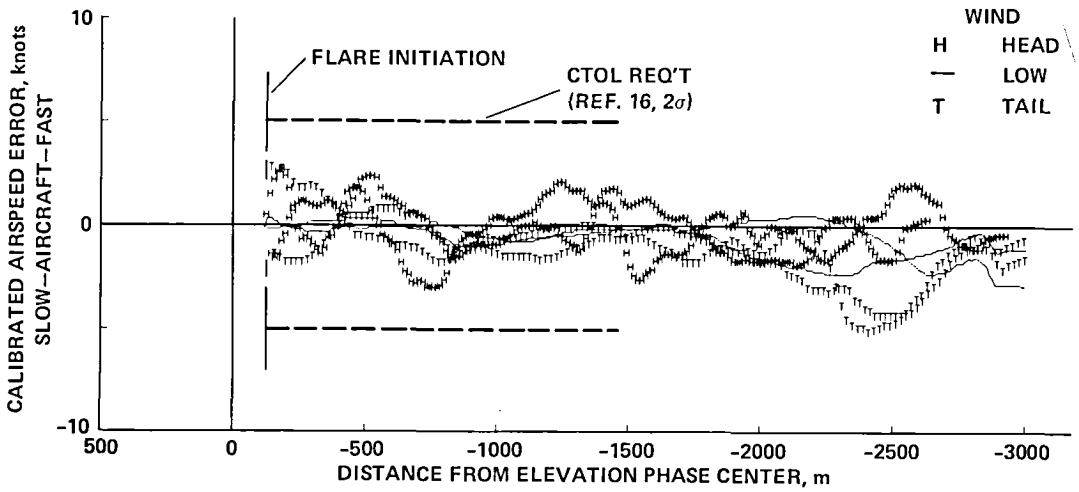

Figure 15.– Typical variations in calibrated airspeed error.

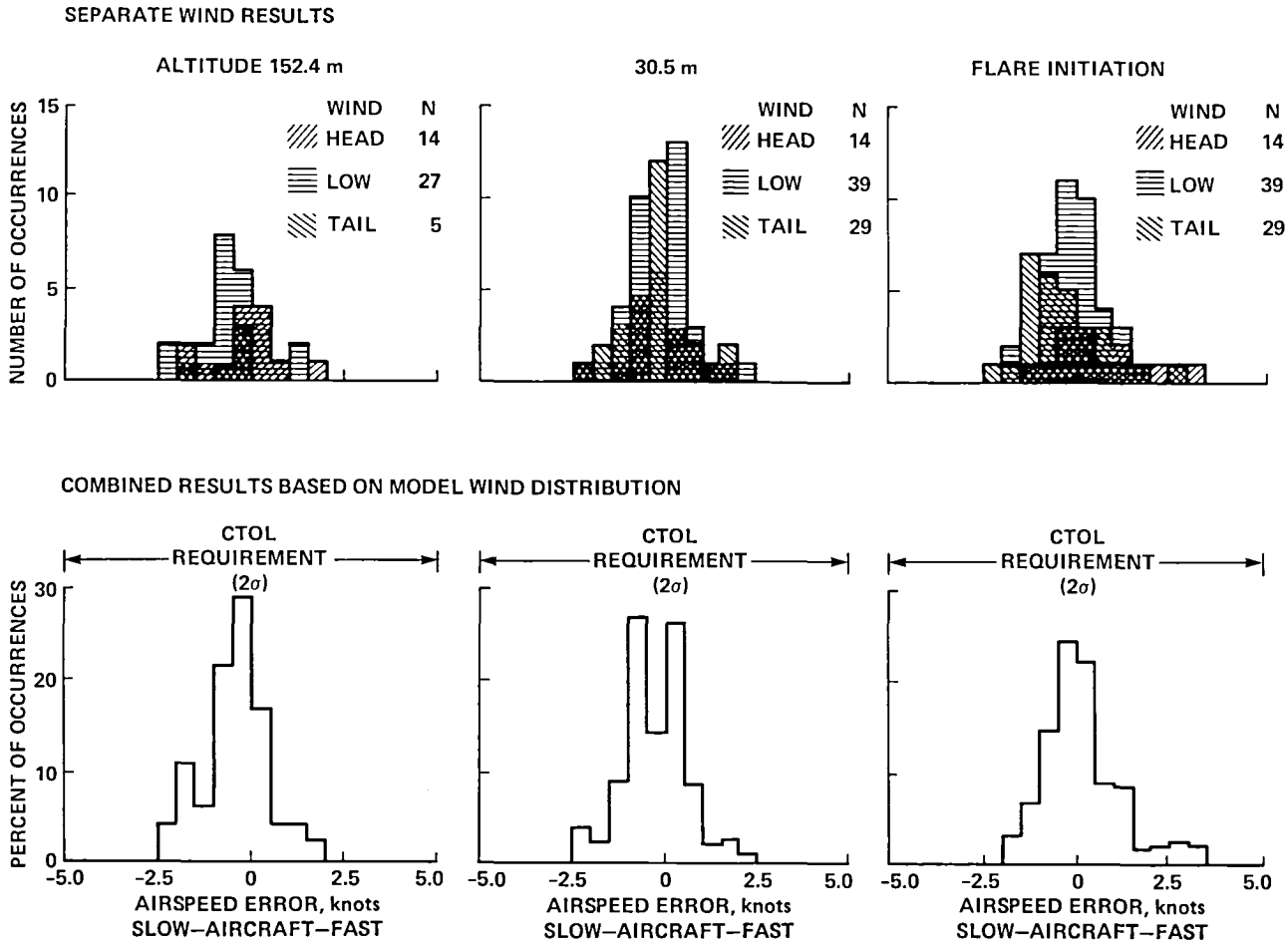

Figure 16.– Distributions of calibrated airspeed errors at three altitudes.

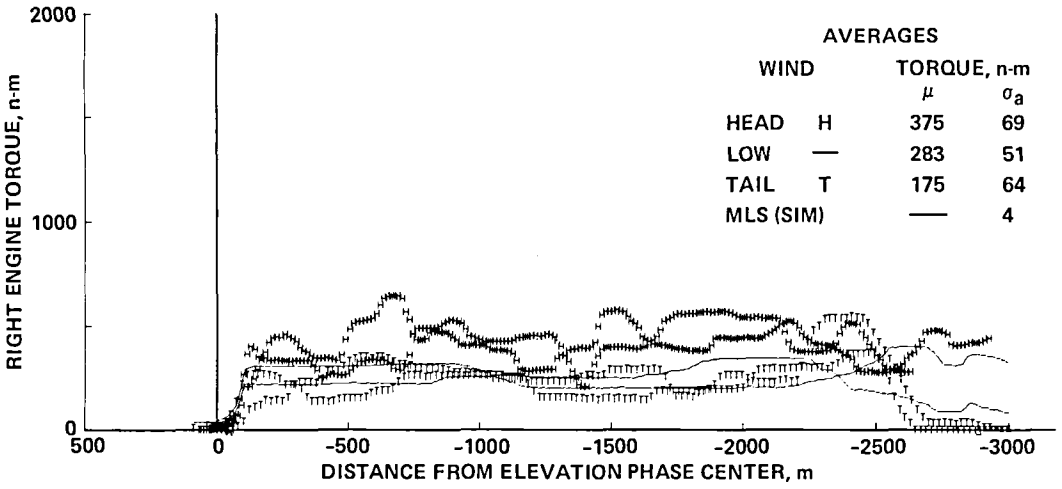

Figure 17.– Typical variations and statistical averages for engine torque.

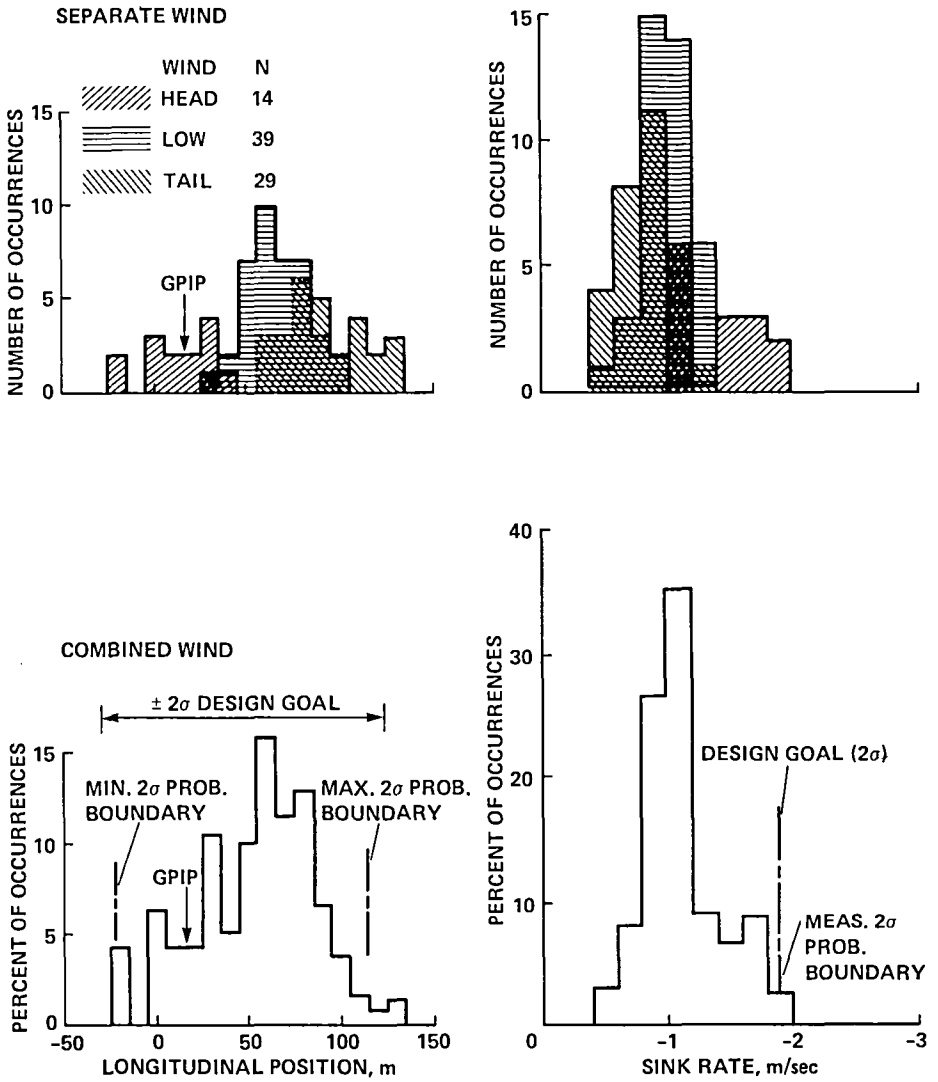

(a) Radar-measured longitudinal position from elevation phase center and onboard-measured sink rate.

Figure 18.– Distributions at touchdown from flight measurements.

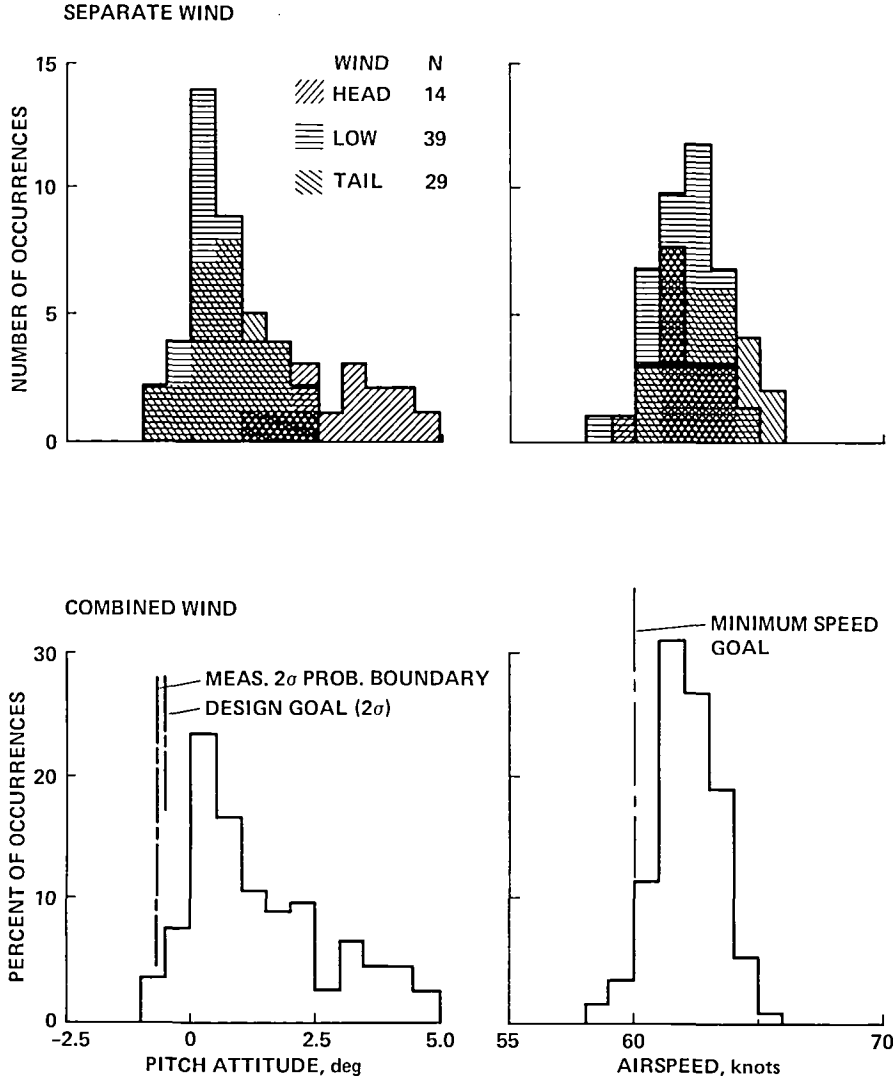

(b) Pitch attitude and calibrated airspeed.

Figure 18.– Concluded.

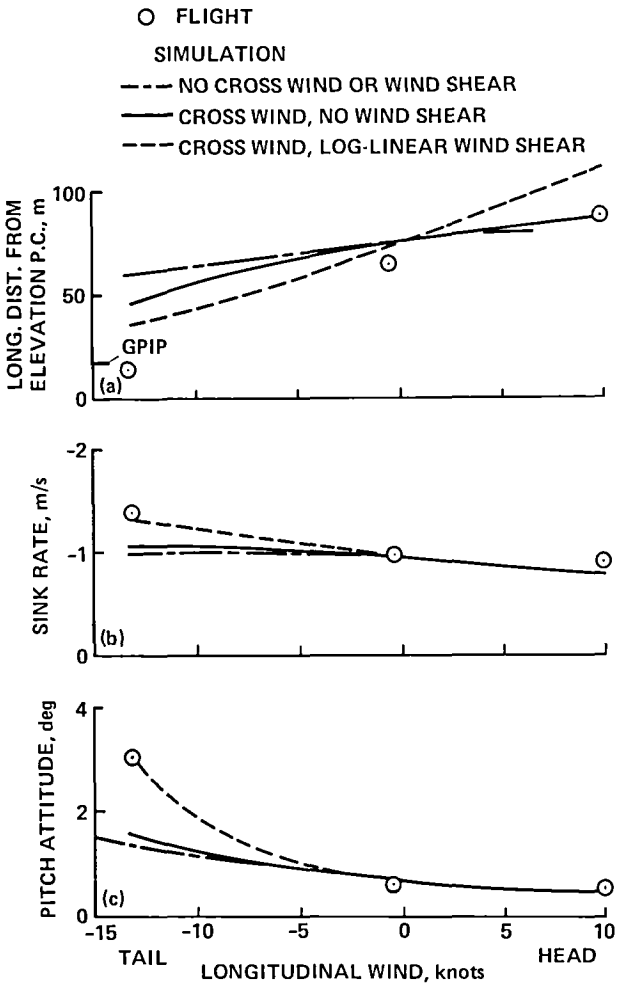

Figure 19.– Effect of wind on touchdown results from flight and simulation (longitudinal wind from average over 152.4- to 30.5-m altitude range).

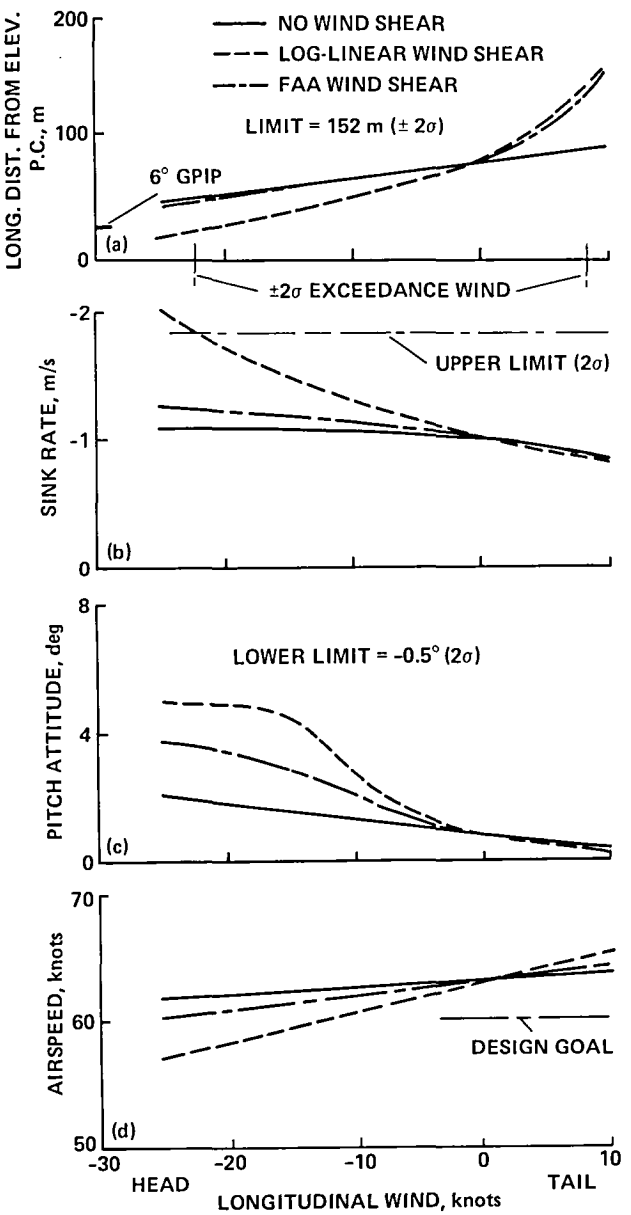

Figure 20.– Effect of wind on touchdown results from simulation (longitudinal wind at 7.6 m above runway).

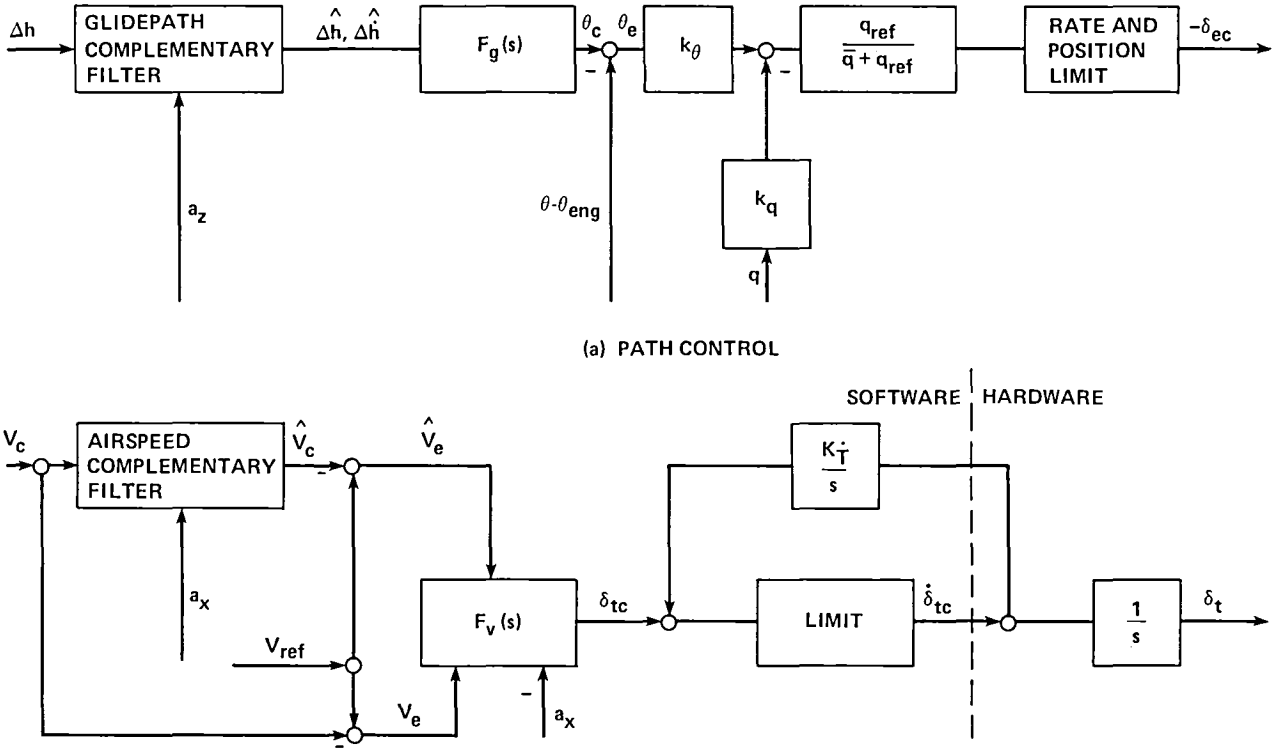

Figure A1.– Final approach control laws.

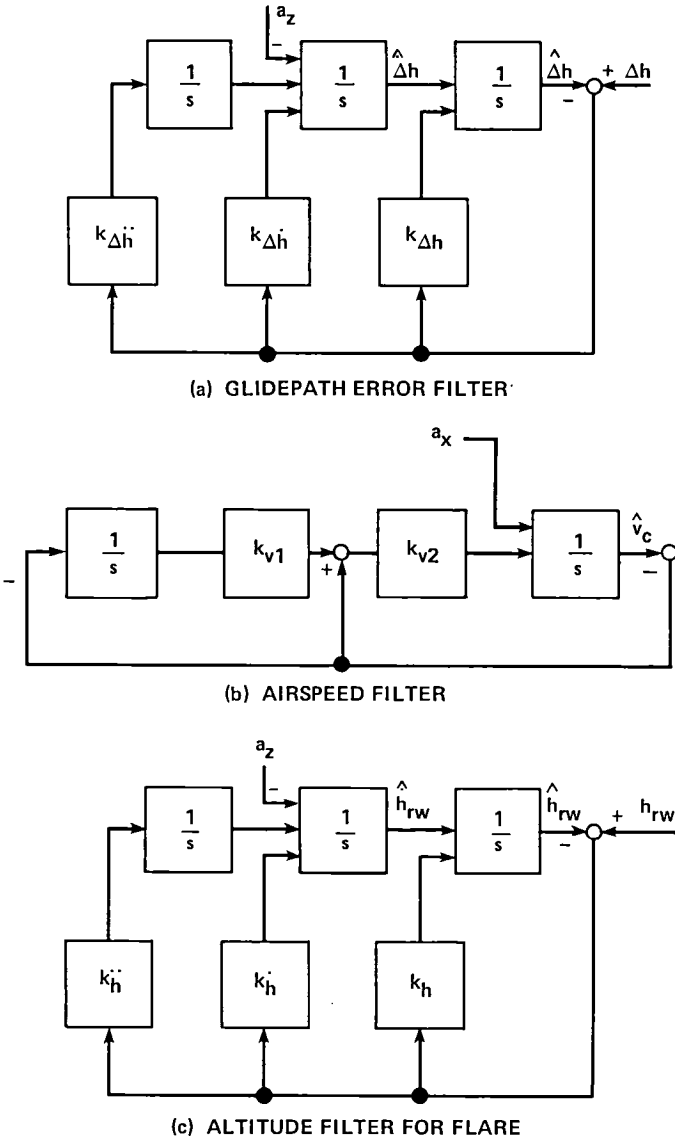

Figure A2.– Vertical and airspeed complementary filters for final approach and flare.

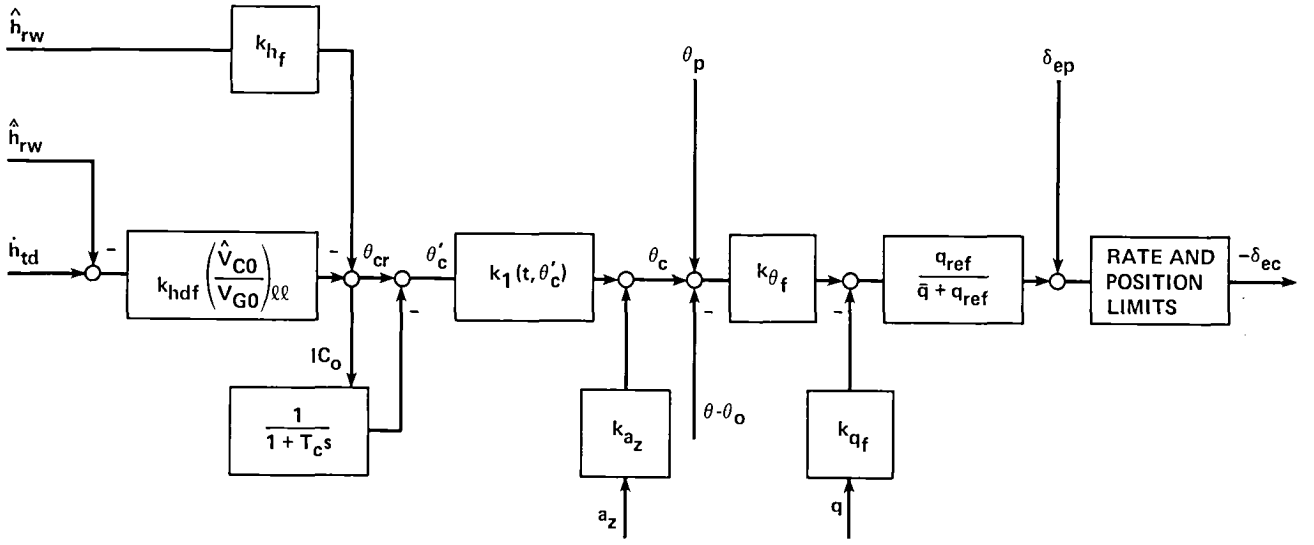

(a) Path and pitch attitude control.

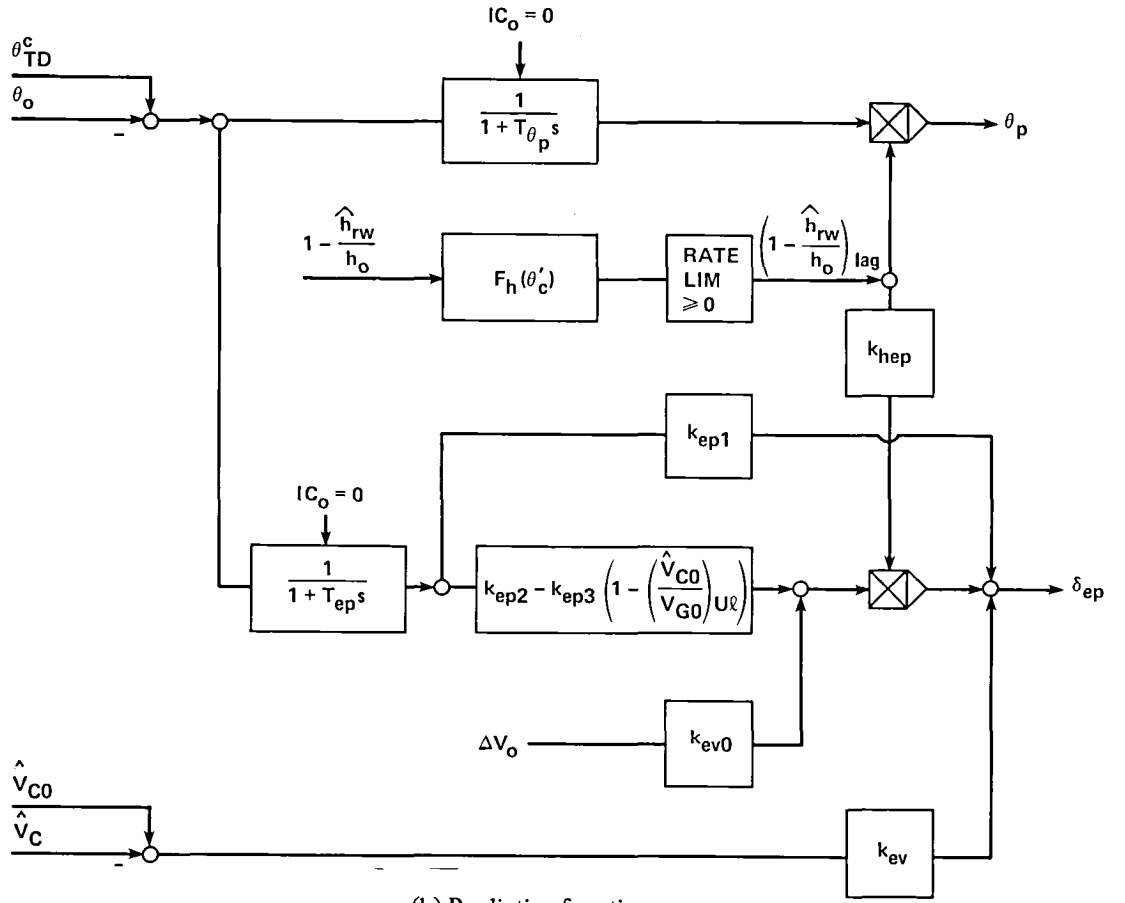

(b) Predictive functions.

Figure A3.– Flare control law.

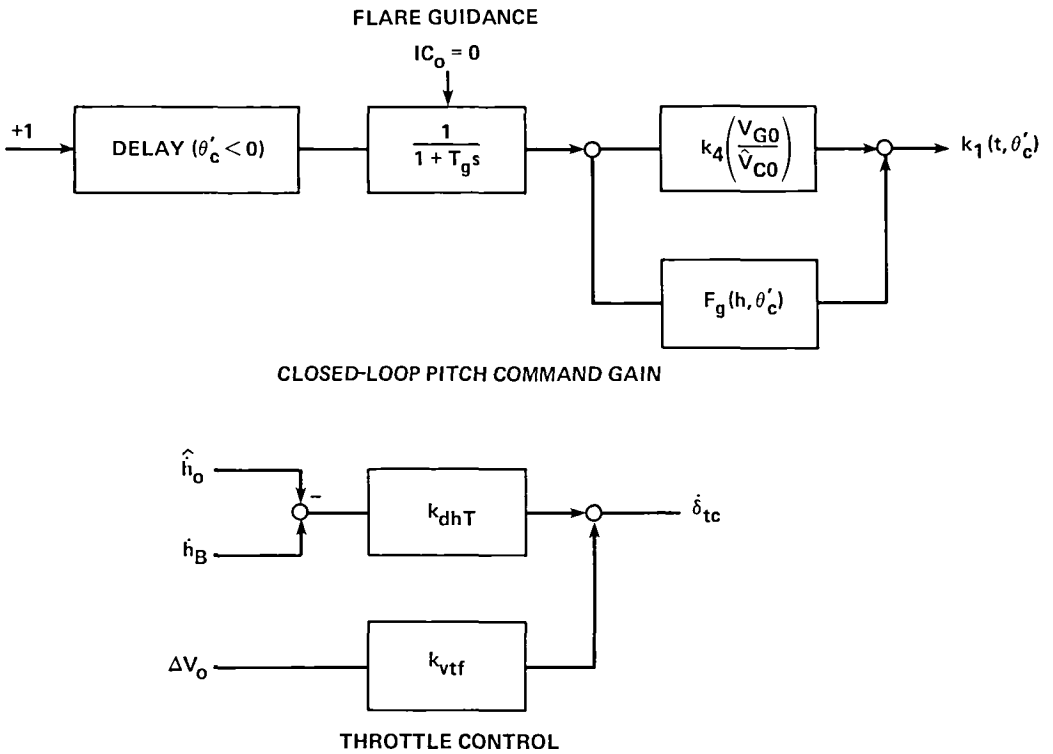

(c) Closed-loop pitch command gain and throttle control.

Figure A3.– Concluded.

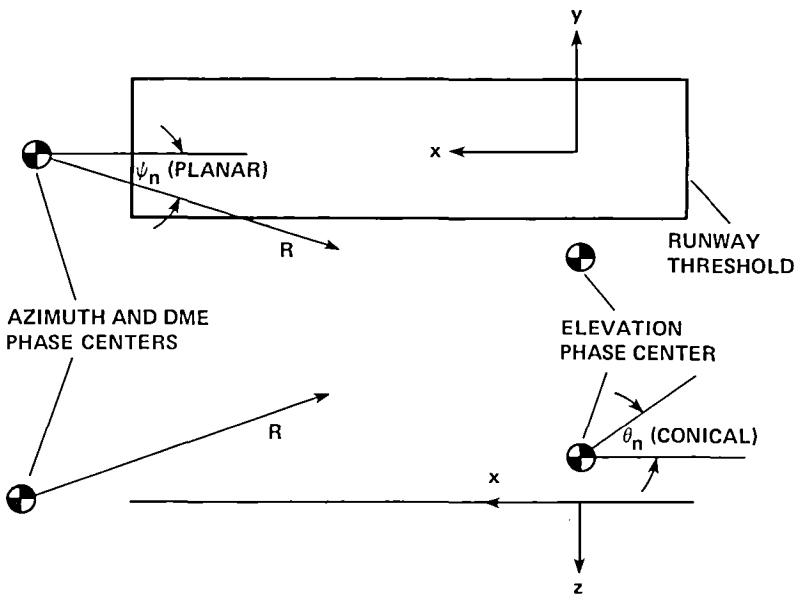

Figure A4.– MLS and rectangular coordinate systems.

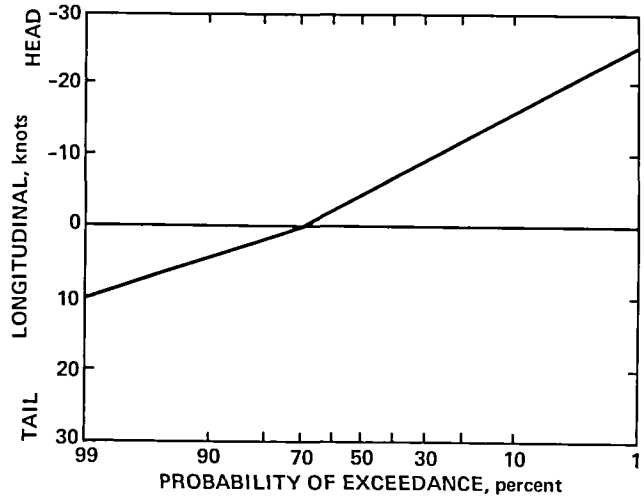

Figure C1.– Wind distribution model.

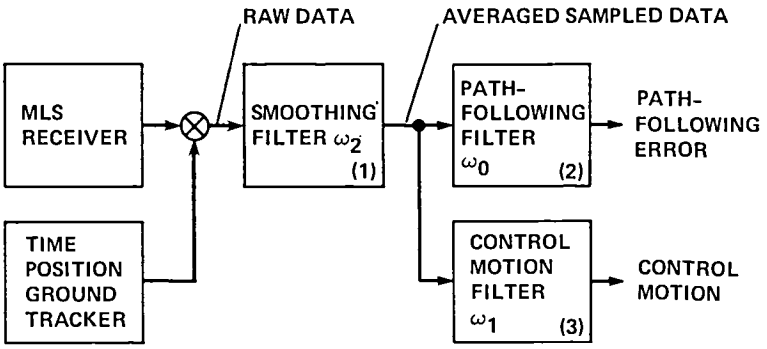

BLOCK (1) FILTER SMOOTHS SAMPLED DATA. OUTPUT OF FILTER IS VIEWED AS THE OUTPUT OF THE MLS RECEIVER WHICH CAN BE APPROXIMATED BY A FIRST-ORDER FILTER.

BLOCK (2) PATH-FOLLOWING FILTER OUTPUT IS PERTURBATIONS AIRCRAFT WILL TRACK. THESE FLUCTUATIONS FALL WITHIN THE LOOP GUIDANCE BANDWIDTH.

BLOCK (3) CONTROL MOTION RESPONSE FILTER OUTPUT IS NOISE FLUCTUATIONS WHICH AFFECT AIRCRAFT ATTITUDE, CONTROL SURFACE MOTION, COLUMN MOTION, AND WHEEL MOTION.

GUIDANCE FUNCTION	CORNER FREQUENCIES, rad/sec		
	ω_0	ω_1	ω_2
EL	1.0	0.5	10
DME	2.0	0.5	10

FILTER CONFIGURATIONS

SMOOTHING FILTER $\dfrac{\omega_2}{s+\omega_2}$

PATH-FOLLOWING FILTER $\dfrac{\omega_o^2}{(s+\omega_o)^2}$

CONTROL MOTION FILTER $\dfrac{s}{s+\omega_1}$

Figure D1.– MLS specification filters.

1. Report No.	2. Government Accession No.	3. Recipient's Catalog No.
NASA TM-84270		

4. Title and Subtitle	5. Report Date
A FLIGHT-TEST AND SIMULATION EVALUATION OF THE LONGITUDINAL FINAL APPROACH AND LANDING PERFORMANCE OF AN AUTOMATIC SYSTEM FOR A LIGHT WING LOADING STOL AIRCRAFT	June 1983
	6. Performing Organization Code
7. Author(s)	8. Performing Organization Report No.
Stuart C. Brown, Gordon H. Hardy, and William S. Hindson	A-8993
	10. Work Unit No.
9. Performing Organization Name and Address	T-3848Y
NASA Ames Research Center Moffett Field, Calif. 94035	11. Contract or Grant No.
	13. Type of Report and Period Covered
12. Sponsoring Agency Name and Address	Technical Memorandum
National Aeronautics and Space Administration Washington, D.C. 20546	14. Sponsoring Agency Code 532-02-11

15. Supplementary Notes

Point of contact: Gordon H. Hardy, Ames Research Center, MS 211-3, Moffett Field, Calif. 94035
(415)965-5278 or FTS 448-5278

16. Abstract

As part of a comprehensive flight-test program of STOL operating systems for the terminal area being conducted at the NASA Ames Research Center, an automatic landing system has been developed and evaluated for a light wing loading turboprop aircraft. The aircraft utilized an onboard advanced digital avionics system. Flight tests were conducted at a facility that included a STOL runway site with a microwave landing system.

Longitudinal flight-test results were presented and compared with available (basically CTOL) criteria. These comparisons were augmented by results from a comprehensive simulation of the controlled aircraft which included representations of navigation errors that were encountered in flight and atmospheric disturbances.

Acceptable performance on final approach and at touchdown was achieved by the autoland (automatic landing) system for the moderate winds and turbulence conditions encountered in flight. However, some touchdown performance goals were marginally achieved, and simulation results suggested that difficulties could be encountered in the presence of more extreme atmospheric conditions. Suggestions were made for improving performance under those more extreme conditions.

17. Key Words (Suggested by Author(s))	18. Distribution Statement
Light wing loading STOL aircraft Automatic digital flight control Automatic landing system	Unclassified - Unlimited Subject Category – 08

19. Security Classif. (of this report)	20. Security Classif. (of this page)	21. No. of Pages	22. Price*
Unclassified	Unclassified	59	A04

*For sale by the National Technical Information Service, Springfield, Virginia 22161

NASA-Langley, 1983